Available online at www.sciencedirect.com

ScienceDirect

Geochimica et Cosmochimica Acta 218 (2017) 114–131

Geochimica et Cosmochimica Acta

www.elsevier.com/locate/gca

Stepwise heating of lunar anorthosites 60025, 60215, 65315 possibly reveals an indigenous noble gas component on the Moon

David V. Bekaert [a,*], Guillaume Avice [a,1], Bernard Marty [a], Bryana Henderson [b], Murthy S. Gudipati [b]

[a] *Centre de Recherches Pétrographiques et Géochimiques, CRPG-CNRS, Université de Lorraine, UMR 7358, 15 rue Notre Dame des Pauvres, BP 20, 54501 Vandoeuvre-lès-Nancy, France*

[b] *Science Division, Jet Propulsion Laboratory, California Institute of Technology, 4800 Oak Grove Dr, Pasadena, CA 91109, USA*

Received 3 September 2016; accepted in revised form 29 August 2017; available online 8 September 2017

Abstract

Despite extensive effort during the last four decades, no clear signature of a lunar indigenous noble gas component has been found. In order to further investigate the possible occurrence of indigenous volatiles in the Moon, we have re-analyzed the noble gas and nitrogen isotopic compositions in three anorthosite samples. Lunar anorthosites 60025, 60215 and 65315 have the lowest exposure duration (~2 Ma) among Apollo samples and consequently contain only limited cosmogenic (e.g. ^{124,126}Xe) and solar wind (SW) noble gases. Furthermore, anorthosites have negligible contributions of fissiogenic Xe isotopes because of their very low Pu and U contents. As observed in previous studies (Lightner and Marti, 1974; Leich and Niemeyer, 1975), lunar anorthosite Xe presents an isotopic composition very close to that of terrestrial atmospheric Xe, previously attributed to "anomalous adsorption" of terrestrial Xe after sample return. The presumed atmospheric Xe contamination can only be removed by heating the samples at medium to high temperatures under vacuum, and is therefore different from common adsorption. To test this hypothesis, we monitored the adsorption of Xe onto lunar anorthositic powder using infrared reflectance spectroscopy. A clear shift in the anorthosite IR absorbance peaks is detected when comparing the IR absorbance spectra of the lunar anorthositic powder before and after exposure to a neutral Xe-rich atmosphere. This observation accounts for the chemical bonding (chemisorption) of Xe onto anorthosite, which is stronger than the common physical bonding (physisorption) and could account for the anomalous adsorption of Xe onto lunar samples.

Our high precision Xe isotope analyses show slight mass fractionation patterns across $^{128–136}$Xe isotopes with systematic deficits in the heavy Xe isotopes (mostly ^{136}Xe and marginally ^{134}Xe) that have not previously been observed. This composition could be the result of mixing between an irreversibly adsorbed terrestrial contaminant that is mostly released at high temperature and an additional signature. Solar Wind (SW) Xe contents, estimated from SW-Ne and SW-Ar concentrations and SW-Ne/Ar/Xe elemental ratios, do not support SW as the additional contribution. Using a χ^2 test, the latter is best accounted for by cometary Xe as measured in the coma of Comet 67P/Churyumov-Gerasimenko (Marty et al., 2017) or by the primordial U-Xe composition inferred to be the precursor of atmospheric Xe (Pepin, 1994; Avice et al., 2017). It could have been contributed to the lunar budget by volatile-rich bodies that participated to the building of the terrestrial atmosphere inventory (Marty et al., 2017).

Keywords: Moon; Noble gases; Indigenous component; Comets

* Corresponding author.
E-mail address: dbekaert@crpg.cnrs-nancy.fr (D.V. Bekaert).
[1] Present address: California Institute of Technology, Division of Geology and Planetary Sciences, 1200 E California Boulevard, Pasadena, CA 91125, USA.

https://doi.org/10.1016/j.gca.2017.08.041
0016-7037/

1. INTRODUCTION

Terrestrial-like isotopic compositions of refractory and volatile elements measured in lunar samples have raised important questions concerning the formation of the Earth–Moon system (e.g., Dauphas et al., 2014). Several key observables, such as (i) the high angular momentum between the two bodies, (ii) the Moon's abnormally large size relative to its host planet, (iii) the delayed formation of the Moon relative to Earth, up to ~95 Myrs after the birth of the solar system (Jacobson et al., 2014), and (iv) the depletion of key volatiles and iron in the Moon (Ganapathy and Anders, 1974; Elliott and Stewart, 2013), have been interpreted as evidence for a common origin from a violent impact (e.g. Hartmann and Davis, 1975; Canup and Esposito, 1996; Canup, 2004a,b, 2013; Hiesinger and Head, 2006; Ćuk and Stewart, 2012; Elliott and Stewart, 2013). However, most numerical models of lunar-forming impacts predict that the Moon is mainly made of the impactor material (e.g., Canup, 2013; Canup et al., 2013), which is at odds with the terrestrial-like isotopic compositions of oxygen (Wiechert, 2001), silicon (Armytage et al., 2012), calcium (Simon and DePaolo, 2010), magnesium (Sedaghatpour et al., 2013), iron (Moynier et al., 2006), titanium (Zhang et al., 2012), strontium (Moynier et al., 2010) and chromium (Lugmair and Shukolyukov, 1998) of lunar samples. Thus, either the material from the proto-Earth and the impactor were thoroughly homogenized (Pahlevan and Stevenson, 2007; Elliott and Stewart, 2013; Young et al., 2016) or the impactor had an Earth-like isotopic composition (Meier et al., 2014; Dauphas et al., 2014). Even if unclear (Genda and Abe, 2005), the giant impact that formed the Moon would have removed a significant portion of the proto-Earth's atmosphere and thus the Earth would have started to retain its actual atmosphere after formation of the Earth–Moon system. A common origin for Earth–Moon materials would thus have important implications for the origin and early evolution of the Earth's atmosphere. The lunar volatile budget would represent a proxy for the external contributions to the Earth's volatile inventory after the Earth–Moon formation, e.g., during the Late Veneer and/or during the Late Heavy Bombardment (LHB) 4.0–3.8 Gyr ago (Hartmann et al., 2002; Morbidelli et al., 2012; Bottke et al., 2012). While traces of such bombardment episodes are seen on the present-day surface of the Moon (Ong et al., 2010; Bogard, 2011), no evidence for such a contribution to the lunar noble gas budget has been detected from analyses of lunar samples. More generally, no indigenous noble gas component has been found on the Moon despite extensive searches (Wieler and Heber, 2003).

Lunar noble gases are mostly of solar wind (SW) origin. Minute amounts of terrestrial-like noble gases have been released from lunar samples at low temperature during stepwise heating, and their origin was attributed to physical adsorption of a terrestrial component. However, terrestrial-like Xe was also released at medium to high temperatures (>1000 °C) from lunar anorthosites (Lightner and Marti, 1974; Leich and Niemeyer, 1975; Eugster, 1986), a behavior attributed to "irreversible" adsorption. Subsequent experiments confirmed this by exposing crushed samples to an artificial Xe-rich atmosphere (Niemeyer and Leich, 1976). Furthermore, samples crushed under atmospheres enriched in certain isotopes of xenon and krypton showed pressure-dependent enrichments of these isotopes (Niedermann and Eugster, 1992). This anomalous adsorption appeared to be more efficient for Xe than for Kr by about one order of magnitude, possibly due to mechanical forces during crushing or labyrinth porosity effects, which would have delayed the release of the terrestrial contaminant. The common physisorption of noble gases onto surfaces, due to Van der Wals forces induced from mutual electric dipole induction (Ozima and Podosek, 2002; Marrocchi and Marty, 2013), leads to outgassing of the volatiles at their sublimation temperature, which is ~70 K for Xe under vacuum. Thus, this mechanism cannot account for the high release temperature of Xe (Leich and Niemeyer, 1975; Niemeyer and Leich, 1976). Recently, it has been shown that even atmospheric helium can be adsorbed in large quantities onto the surface of mineral grains and that very high temperatures are required (>900 °C) to release this adsorbed component (Protin et al., 2016). In order to investigate the possible occurrence of chemical interactions between noble gases and solid surfaces, we monitored Xe adsorption experiments on lunar anorthositic powder using infrared reflectance spectroscopy (Clark et al., 1990; Thomson and Salisbury, 1993). High-energy sites generated during crushing of the samples could induce chemical interactions between heavy noble gases and new active surfaces (Garrison et al., 1987; Hohenberg et al., 2002; Marrocchi et al., 2011). In such case, the IR absorbance peaks of the anorthositic powder should shift, between the processed (i.e. exposed to Xe gas) and unprocessed absorbance spectra, where Xe atoms are chemically bonded to atoms at the anorthosite grain surface.

We also carried out a complete noble gas and nitrogen isotope study of three lunar cataclastic anorthosite chips (60025.817, 60215.48 and 65315.142), in two sets of experiments, an induction furnace stepwise heating session and a series of laser extractions. Our aim was to test if the terrestrial-like isotopic composition of the adsorbed Xe (Lightner and Marti, 1974; Leich and Niemeyer, 1975) could be verified at high precision, i.e. at the part per thousand level (given as per mil, noted ‰), computed in delta notation as:

$$\delta^{i}\mathrm{Xe}\ (‰) = \left(\frac{(^{i}\mathrm{Xe}/^{132}\mathrm{Xe})_{\mathrm{sample}}}{(^{i}\mathrm{Xe}/^{132}\mathrm{Xe})_{\mathrm{atm}}} - 1 \right) * 1000 \quad (1)$$

where δ^{i}Xe is the deviation of the sample $^{i}Xe/^{132}Xe$ ratio from the terrestrial atmosphere value.

2. SAMPLES

The identification of a noble gas indigenous component in lunar samples is particularly challenging as external contributions from the solar wind (Wieler et al., 1986; Pepin et al., 1995) and/or cosmic rays (Reedy and Arnold, 1972; Hohenberg et al., 1978) may have affected the noble gas budget of lunar rocks exposed to space at the lunar surface.

We analyzed three lunar anorthosite samples characterized by low exposure durations, thus minimizing the corrections required for contributions from cosmogenic noble gases (Leich and Niemeyer, 1975; Niedermann and Eugster, 1992). The three samples consisted of coarse-grained granular cataclastic chips (James, 1980) returned to Earth by the Apollo 16 NASA mission in 1972. Their exposure ages cluster between 1.5 and 2 Ma (see Arvidson et al. (1975) and Drozd et al. (1977) for sample 60025, Eugster (1999) for sample 60215 and Stettler et al. (1974), Eberhardt et al. (1975), Gopalan and Rao (1976) and Eugster et al. (1984) for sample 65315), interpreted as evidence for excavation during the South Ray cratering event 2 Myr ago (Eugster, 1999). Before excavation, these samples were presumably shielded from interactions with cosmic-ray particles. Sample 65315, a monomictic cataclastic ferroan and chemically pristine anorthosite (Meyer, 2012), is the least shocked of the three samples. Sample 60215 is a predominantly monomictic highly shocked breccia, displaying very low porosity, impact melts and a vesicular glass coating (Meyer and McCallister, 1973; Meyer, 2012). Sample 60025 is a moderately shocked, chemically pristine and coarse-grained anorthosite (Meyer, 2011). The grains analyzed in our study corresponded to few hundred milligrams of fresh interior chips, obtained from the surface (60215.48) and the sub-surface (65315.142) of the parent rock. As expected from their pristine anorthositic mineralogy, very low concentrations of large ion lithophilic elements—the parents of Xe heavy isotopes through fission processes—are present in these samples (Lightner and Marti, 1974). The U contents were found to be below the 0.1 ppm detection limit of the Service d'Analyse des Roches et des Minéraux (SARM, CRPG Nancy, France, see Table A1 in Appendix A). Likewise, very low Ba and REE contents—the main target elements for Xe cosmogenic production by spallation—were measured at SARM ([Ba] $\leq$ 11 ppm and [La] $<$ 0.4 ppm, see Table A1 in Appendix A).

3. EXPERIMENTAL PROCEDURES

In order to minimize potential atmospheric contamination during sample preparation, we selected the largest pieces available that fitted the dimensions of the samples holders. Two samples of 65315.142 (m_{tot} = 534.8 mg), three of 60215.48 (m_{tot} = 391 mg) and two of 60025.817 (m_{tot} = 297.8 mg), all a few millimeters in size, were handpicked. These samples were reserved for Ar, Kr and Xe isotopic measurements by stepwise heating in an induction furnace (Zimmermann and Marty, 2014). Single grains of 65315.142 (5.034 mg), 60215.48 (4.198 mg) and 60025.817 (a: 2.014 mg and b: 5.281 mg) were handpicked for He, Ne, Ar and N_2 isotopic analyses by CO_2 laser extraction followed by static mass spectrometry (Humbert et al., 2000). Error propagation for isotopic analyses is detailed in Appendix B.

3.1. Induction furnace extraction

Samples were handled in a clean room at CRPG Nancy (France). To minimize contamination, the samples were not cleaned with solvents or water. Large (several mm) blocks were loaded into the sample holder without metal wrapping in order to minimize blank contributions. Seven pieces of anorthosite were stored inside the glass part of the induction furnace under high vacuum (10^{-9} mbar) at 120 °C for two days in order to degas weakly bound atmospheric gases. A temperature step at 400 °C was applied first using a quartz oven. Individual samples were then moved using a magnet and an iron stick and dropped into the Ta crucible of the induction furnace, where 850 °C, 1400 °C, 1800 °C and 2000 °C temperature steps of 20 min each were applied. To reach the plateau temperature, the power supply was increased slowly, corresponding to temperature increments of ~60 °C/5 min, from a starting temperature of 700 °C, in order to avoid damaging the glass part of the extraction system. Likewise, the temperature was reduced at a similar rate after the extraction step. For the 1800 °C step, the complete sequence took ~4 h. For all temperature steps except the 2000 °C step, blank contributions were in the range 0.2–20% for ^{36}Ar, 1.2–8% for ^{84}Kr and 0.05–1.3% for ^{132}Xe (see Tables A4–A6 in Appendix A). Samples were observed to melt at temperatures up to 1800 °C, and thus the final 2000 °C extraction step was carried out in order ensure that all of the gas had been extracted from the samples. While the temperature of 400 °C is fairly precise (as it was directly measured with a thermocouple), the higher temperatures were measured with an optical pyrometer and are thus only indicative (±100 °C). Series of standards and blanks were run between each sample each day for subsequent blank and spectrometer mass discrimination corrections (see Appendix B). No deviation in the standard isotopic ratios was detected over the periods of analysis. Extracted gases were purified using Ti-sponge getters held at 650 °C for 5 min and then cooled down to room temperature over the next 5 min. Xe and Kr were separated from Ar on the surface of a Pyrex finger held at liquid nitrogen temperature for 20 min. Around 75% of the Kr and >95% of Xe atoms were thus isolated from the rest of the purification system. Argon isotopic measurements were carried out on the remaining fraction first. The partial pressure of Ar in the volume of the glass finger was then reduced by diluting 10 times the volume of the cold finger, still at liquid nitrogen temperature, into the whole line. During pumping of the line, the glass finger held at liquid nitrogen temperature was isolated from the line. Finally, the glass trap (containing the Xe and Kr) was heated up and the gas released was exposed once again to two other hot Ti-sponge getters for final purification. Krypton and xenon isotopes were measured with a Helix MC Plus (Thermofisher Scientific@) mass spectrometer by peak jumping on the central compact dynode electron multiplier AX (CDD).

3.2. CO_2 laser extraction

Helium, neon, argon and nitrogen were extracted by heating the samples with a CO_2 infrared (λ = 10.6 μm) laser (Humbert et al., 2000). The power supplied to the laser was modulated in order to attain a first extraction step at low temperature (~600 °C) and a second extraction step over the melting point of the sample (>1600 °C). The first extrac-

tion temperature was estimated qualitatively by stopping the increase in the laser power as soon as the heated sample turned reddish. The formation of a spherule of molten silicate during the second temperature step indicated that the melting temperature of the sample had been reached, and that more than 99% of the gas had been extracted (Humbert et al., 2000). Extracted gases were then split into two calibrated volumes for separate purification and analysis. Nitrogen and noble gases were analyzed with a VG5400 mass spectrometer (Hashizume and Marty, 2004; Zimmermann et al., 2009 and Füri et al., 2015). The respective blanks were 6.3×10^{-16} mol ^{4}He, 3.3×10^{-17} mol ^{22}Ne, 2.6×10^{-17} mol ^{36}Ar and 6.9×10^{-13} mol $^{28}N_2$.

3.3. Infrared reflectance spectroscopy

At the Jet Propulsion Laboratory (Pasadena, USA), we carried out Xe adsorption experiments onto lunar anorthositic powder monitored by infrared reflectance spectroscopy (Clark et al., 1990; Thomson and Salisbury, 1993) using a Thermoscientific Nicolet 6700FT-IR Spectrometer. The lunar anorthosite powder was loaded onto a stainless-steel sample holder positioned behind a KBr window, which is transparent to a wide range of infrared wavelengths (Stuart, 2005; See Fig. C1 in Appendix C). The sample chamber was evacuated to reach a final pressure of $\leq 10^{-6}$ mbar. The anorthosite powder consisted of a naturally disintegrated portion of lunar sample 60215 (consisting of micron- to hundreds of micron sized grains) contained at the bottom of the storage holder and thus no particular crushing was required for the experiment. The sample holder was placed at the focal point of two parabolic gold-plated mirrors. The first mirror was used to focus the collimated infrared beam coming from a flat gold-plated mirror set in front of the modulated beam output of the Fourier Transform InfraRed (FTIR) spectrometer. The second mirror collected the diffuse infrared light reflected from the surface of the sample, while another flat gold-plated mirror steered the diffuse infrared light toward a final parabolic gold-plated mirror that focused the diffuse beam on to the detector (See Fig. C1 in Appendix C). The obtained signal was maximized by adjusting the orientation of each mirror along with the height of the sample holder. This experimental method is commonly used for the infrared spectroscopic analysis of solid samples, also known as Reflection-Absorption Infrared (RAIR) Spectroscopy (e.g., Hoffmann, 1983). In this method, a reference reflectance spectrum is measured before or after a sample reflectance spectrum. Using these two single-beam spectra, the absorbance spectrum of the sample is calculated. If two such sample spectra were measured without external changes to the optical components, the difference in these two spectra can quantitatively be attributed to structural changes of the powder sample. We followed this method to investigate spectral changes due to Xe adsorption on lunar anorthosite. Analyzed wavelengths ranged from the near to mid-infrared region, from 1.25 μm to 25 μm (400–8000 cm^{-1}). Reference infrared reflectance spectra of the stainless-steel sample holder were measured without anorthosite powder and found to be consistently identical. The anorthosite powder was then spread onto the sample holder and the sample chamber was evacuated to $\leq 10^{-6}$ mbar. Subsequently, the infrared reflectance spectrum of the anorthosite (sample) was measured. From the reflectance spectra of the stainless-steel sample holder (reference) and anorthositic powder (sample), we calculated the RAIR absorbance spectrum of the anorthosite as:

$$\mathrm{Abs} = -\log\left(\frac{\mathrm{Refl}_{\mathrm{powder}}}{\mathrm{Refl}_{\mathrm{support}}}\right) \quad (2)$$

where $\mathrm{Refl}_{\mathrm{powder}}$ and $\mathrm{Refl}_{\mathrm{support}}$ are the reflected wavelength-dependent radiant fluxes (arbitrary unit) measured from the stainless-steel sample holder with and without the anorthosite powder, respectively. As infrared spectroscopy relies on the absorbance of radiation at molecular vibrational frequencies, each positive peak at a given wavelength of the resulting absorbance spectra indicates that molecules from the anorthositic powder are absorbing the IR light at this wavelength. Subsequently, the anorthosite powder sample under vacuum (10^{-6} mbar) was exposed to a pure Xe by letting pure Xe slowly flowing through a dosing needle valve until the pressure reached 500 mbar. The anorthosite powder sample was kept under the 500 mbar Xe atmosphere for several hours. Following this, we measured the reflectance spectra of these samples under Xe atmosphere. We note that the reflectance spectra (unlike transmittance) are a convolution of real and imaginary indices of refraction as well as scattering due to the sample grains. However, when these samples are not altered by any means other than exposure to Xe atmosphere, any changes in the reflectance spectra should only be due to the interaction of Xe with the sample. In the case of Xe adsorption onto the anorthosite due to physical Van der Waals bonding (physisorption), no shift should be observed. When chemical bonding between the atoms takes place (chemisorption), the corresponding absorbance peaks shift (Hobza and Havlas, 2000). If a chemical interaction occurs between Xe and the anorthosite, the strength of bonding between the functional groups forming the bond with Xe should be reduced, resulting in a shift of the molecule absorbance peak toward the lower wavenumbers (Scheiner, 1997). We investigated and observed the occurrence of such shifts in the anorthosite peaks by comparing the absorption spectra of the lunar anorthosite powder obtained before and after exposure to Xe.

4. RESULTS

4.1. He, Ne, Ar, N_2 and Kr isotopic compositions

4.1.1. Helium

Helium isotope data are given in Appendix A, Table A2. The helium content of sample 65315 is among the lowest ever measured in lunar samples (Niedermann and Eugster, 1992). The ^{3}He/^{4}He ratios of samples 60215.48 and 60025.817 [$9 \cdot 10^{-6}$–$1.6 \cdot 10^{-4}$] are high compared to the ratio of terrestrial atmospheric He ($[^{3}\mathrm{He}/^{4}\mathrm{He}]_{\mathrm{ATM}} \sim (1.382 \pm 0.005) \cdot 10^{-6}$, Sano et al. (2013)) but are lower

than the present-day solar wind ratio ($[^3He/^4He]_{SW} \sim (4.41 \pm 0.23) \times 10^{-4}$, Grimberg et al. (2008)), thus implying a large contribution from spallation-produced ^3He.

4.1.2. Neon

Neon isotopic ratios consistently reflect a three-component mixture between atmospheric (Heber et al., 2009), cosmogenic (Leya et al., 2001) and solar wind-like (Pepin et al., 2012) end-members (Fig. 1, Table A3 in Appendix A). Sample exposure ages are ~0.2 Ma, as calculated from ^{21}Ne data using the calculation model for rates of cosmogenic production by galactic cosmic rays of Leya et al. (2001) and sample chemical compositions obtained at SARM (Table A1, Appendix A), and are thus one order of magnitude lower than published data (~1.5 Ma, Gopalan and Rao (1976), Table 1). This peculiar behavior, as well as the fact that the contributions from the different end-members are indistinguishable upon heating, could be due to the mode of extraction (short duration CO_2 laser heating), which may not warrant thermal equilibrium within the sample.

4.1.3. Argon

Argon isotope data are given in Appendix A, Tables A3 and A4. For the induction furnace heating experiments, our measurements indicate that the radiogenic and cosmogenic (Hohenberg et al., 1978) Ar components, although volume-distributed, are released from the samples at low temperatures: at 400 °C for 60215 and at 850 °C for samples 65315 and 60025 (Fig. 2 for the latter). For the CO_2 laser extraction experiments (Fig. 3), the Ar cosmogenic and radiogenic components were extracted during the high temperature step (Symbol b in Fig. 3). These contrasting extraction profiles could result from the fact that the induction furnace ensures thermal equilibrium, with extractions lasting from 20 min to several hours, while the CO_2 laser heating (~2–3 min) was possibly not long enough to allow the loss of volume-correlated components during the first extraction step. For two of the three samples (60025 and 65315), linear correlations are observed in a three-isotope diagram of argon (Fig. 3). These correlations define mixing lines between the atmospheric component and an intrinsic component composed of cosmogenic and radiogenic ($^{40}K \rightarrow {}^{40}Ar$) contributions. The absence of such a correlation for sample 60215, along with its low noble gas content, could be related to its highly shocked character (Meyer, 2012).

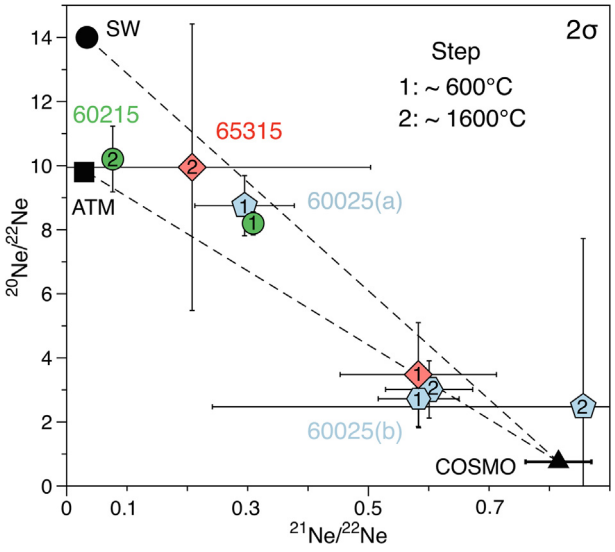

Fig. 1. Isotopic composition of Ne in lunar anorthosites 60025.817 (a and b), 60215.48 and 65315.142 extracted during the CO_2 laser heating experiments. SW: Solar Wind (Pepin et al., 2012), ATM: Terrestrial atmosphere (Heber et al., 2009), Cosmo: Calculated pure cosmogenic component, based on samples chemical composition (Leya et al., 2001). Error bars are 2σ.

Table 1
Cosmogenic exposure ages of samples 65315, 60025 and 60215 from the literature and determined in this study. Exposure ages from ^{21}Ne and ^{38}Ar data were calculated using the calculation model for rates of cosmogenic production by galactic cosmic rays of Leya et al. (2001), assuming a shielding of ~2 cm and using sample chemical compositions obtained at SARM (Table A1, Appendix A). "IF" refers to exposure ages derived from data from the induction furnace while "L" corresponds to the laser heating experiments.

Sample	Exposure age (Ma)	Method	Reference
65315	1.8	^{38}Ar	Stettler et al. (1974)
	1.6	^{38}Ar	Eberhardt et al. (1975)
	1.5 ± 0.7	^{81}Kr	Eberhardt et al. (1975)
	1.5	^{21}Ne	Gopalan and Rao (1976)
	1.3 ± 0.7	^{81}Kr	Eugster et al. (1984)
	1.07	^{38}Ar	This study (IF)
	0.79	^{38}Ar	This study (L)
	0.11	^{21}Ne	This study (L)
60025	1.9	^{81}Kr	Drozd et al. (1977) Arvidson et al. (1975)
	1.90	^{38}Ar	This study (IF)
(a)	1.23	^{38}Ar	This study (L)
(b)	1.21	^{38}Ar	This study (L)
(a)	0.37	^{21}Ne	This study (L)
(b)	0.39	^{21}Ne	This study (L)
60215	2.31 ± 0.5	^{38}Ar	Eugster (1999)
	2.27	^{38}Ar	This study (IF)
	1.43	^{38}Ar	This study (L)
	0.11	^{21}Ne	This study (L)

The K_2O contents of our samples were measured to be below the detection limit of the SARM (CRPG Nancy, France, see Table A1 in Appendix A) and we therefore used the means of the K_2O contents previously reported for these three samples (Meyer, 2011, 2012) to estimate the K-Ar ages of samples 60025 (~4.22 Ga), 65315 (~3.18 Ga) and 60215 (~2.16 Ga). The K-Ar age of 4.22 Ga for sample 60025 is close to ages of 4.360 ± 0.003 Ga determined by Pb-Pb, ^{146}Sm-^{142}Nd and ^{147}Sm-^{143}Nd chronometers (Borg et al., 2011) and is consistent with the ^{40}Ar-^{39}Ar age of 4.18 ± 0.06 Ga given by Schaeffer and Husain (1974). This is in favor of little modified ^{40}Ar contents in this sample, implying limited Ar isotope losses and negligible contributions from implanted ^{40}Ar. Furthermore, and unlike the cosmogenic ^{21}Ne expo-

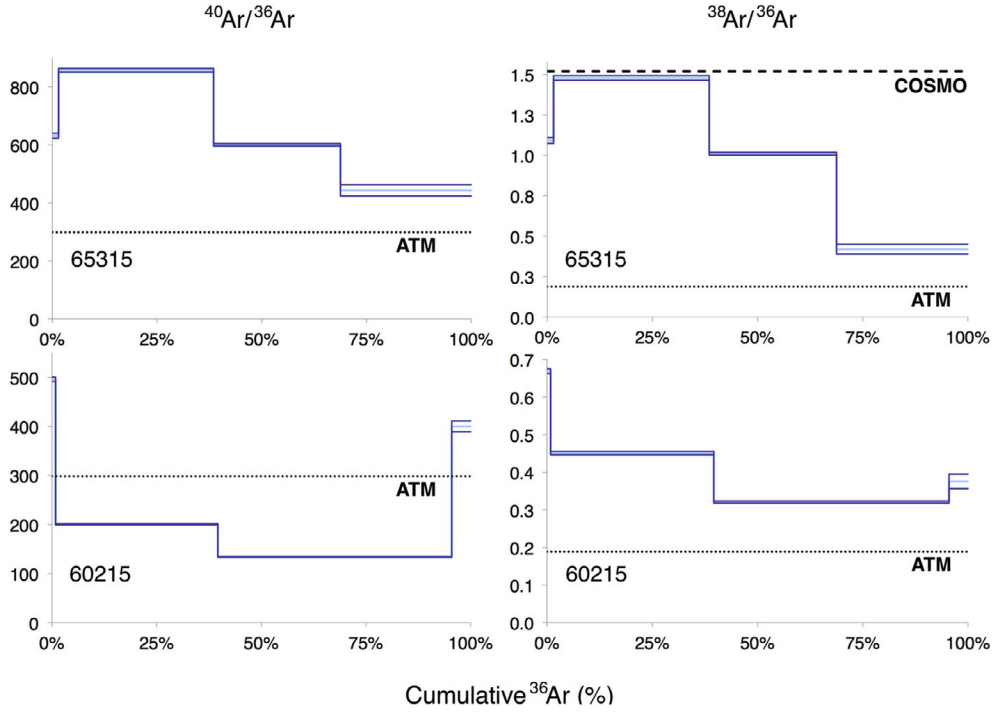

Fig. 2. Argon isotopic composition of lunar anorthosites 65315.142 and 60215.48 (stepwise heating extraction using an induction furnace). The four temperature steps, 400 °C, 850 °C, 1400 °C and 1800 °C are shown as a function of the cumulative ^{36}Ar (%) for each sample. Terrestrial atmosphere (ATM) $^{40}Ar/^{36}Ar$: 298.56, $^{38}Ar/^{36}Ar$: 0.1885 from Lee et al. (2006). Pure cosmogenic (COSMO) $^{40}Ar/^{36}Ar$: 0, $^{38}Ar/^{36}Ar$: 1.52, from Hohenberg et al. (1978). Error bars are 2σ.

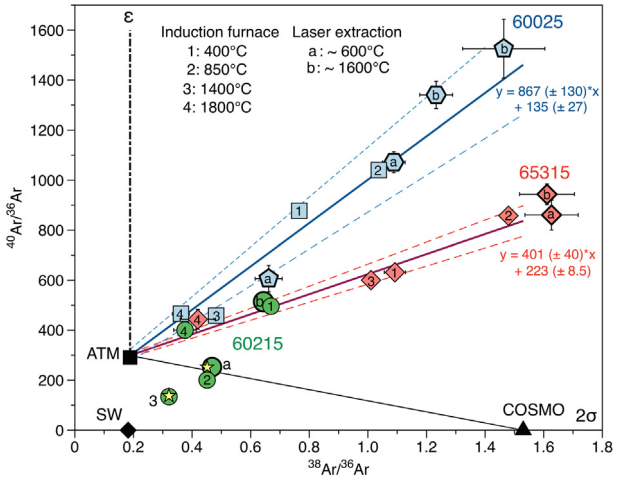

Fig. 3. Argon three-isotope diagram for data for samples 65315, 60025 and 60215 obtained either by induction furnace heating or by CO_2 laser heating. Error bars are 2σ. The solid lines indicate error-weighted correlations and the dashed lines represent their 2σ error envelopes. ε: production of radiogenic ^{40}Ar from ^{40}K by electron capture. Yellow stars are temperature steps 2 and 3 of sample 60215 corrected for a $^{36}Ar_{cosm}$ contribution. Terrestrial atmosphere (ATM) $^{40}Ar/^{36}Ar$: 298.56, $^{38}Ar/^{36}Ar$: 0.1885, from Lee et al. (2006). Pure cosmogenic (COSMO) $^{40}Ar/^{36}Ar$: 0, $^{38}Ar/^{36}Ar$: 1.52, from Hohenberg et al. (1978). (For interpretation of the references to colour in this figure legend, the reader is referred to the web version of this article.)

sure ages, the ^{38}Ar exposure ages are consistent with published data (~2 Ma, Table 1).

The $^{40}Ar/^{36}Ar$ ratios for sample 60215, corrected for a cosmogenic ^{36}Ar contribution, are 252 ± 6 and 138 ± 3 for extraction temperatures of 850 °C and 1400 °C, respectively (*yellow stars,* Fig. 3), both lower than the atmospheric ratio of 298.56 (Lee et al., 2006). Thus, an extra-terrestrial, presumably solar-like, component contributes to the Ar budget of this sample, as is consistent with the Ne isotopic measurements (Fig. 1). Finally, the high temperature steps at 2000 °C released gas abundances similar to the blank values, showing that all trapped gases were released during the 400 °C to 1800 °C temperature steps.

4.1.4. Nitrogen

The samples have low nitrogen contents (~0.14 ppm N_2, Table 2). $\delta^{15}N$ values ($\delta^{15}N = \{[^{15}N/^{14}N]_{sample}/[^{15}N/^{14}N]_{ATM} - 1\} \times 1000$, in parts per mil, where ATM represents terrestrial atmospheric N_2) range between -42.7 ± 55.3‰ and $+45.5 \pm 38.2$‰ and differ from the solar wind value ($\delta^{15}N = -407 \pm 7$‰, Marty et al., 2011). In line with this observation, Füri et al. (2015) analyzed ferroan Anorthosite 15414 using the same extraction method and spectrometer and found no trace of indigenous nitrogen. The present data support their interpretation that nitrogen could have not been retained in the lunar crust during the lunar magma ocean differentiation (Füri et al., 2015). Most likely, the nitrogen detected in our measurements thus corresponds to an adsorbed atmospheric component. Alternatively, this component might have a

Table 2
Nitrogen abundances and isotopic compositions of lunar anorthosites 60025.817, 60215.48 and 65315.142, extracted by CO_2 laser heating. MT° and HT° correspond to the medium temperature (~600 °C) and high temperature (~1600 °C) extraction steps, respectively. Errors are 2σ. For each sample, the two given data are respectively the low temperature and the melting step. The data given for the sample 65315.142 corresponds to a re-extraction at higher temperature. bdl = below detection limits. n.d.: not determined. ^{15}N blank (mol): $6.86.10^{-13}$.

Laser	Extraction step	^{28}N (mol·g^{-1})	+/−	$\delta^{15}N$	+/−
60025.817 (a)	MT°	4.51E−09	4.98E−10	22.8	102.1
(2.014 mg)	HT°	4.07E−09	4.86E−10	−42.7	55.3
	Total	8.58E−09	9.84E−10		
60025.817 (b)	MT°	5.23E−09	3.30E−10	−4.3	54.3
(5.281 mg)	HT°	2.78E−09	2.25E−10	15.0	24.9
	Total	8.01E−09	5.55E−10		
60215.48	MT°	1.04E−09	2.14E−10	13.7	83.7
(4.198 mg)	HT°	1.91E−09	2.32E−10	45.5	38.2
	Total	2.95E−09	4.46E−10		
65315.142	MT°	2.00E−09	2.05E−10	n.d.	–
(5.034 mg)	HT°	1.87E−09	2.01E−10	32.6	56.2
	HT° #2	bdl	–	–	–
	Total	3.87E−09	4.06E−10		

secondary origin (not indigenous) and could have been incorporated during the impact of carbonaceous chondritic material that brecciated the lunar crust (Füri et al., 2015).

4.1.5. Krypton

Concerning krypton (Fig. 4, Table A5 in Appendix A), the pure cosmogenic end-member labeled COSMOc ($^{82}Kr/^{84}Kr$: 1.112, $^{83}Kr/^{84}Kr$: 1.276) is calculated from the chemical composition of the samples (Table A1 in Appendix A) and the cosmogenic production rates of Hohenberg et al. (1978). COSMOa ($^{82}Kr/^{84}Kr$: 2.25 ± 1.44, $^{83}Kr/^{84}Kr$: 3.13 ± 1.95) corresponds to the average lunar bulk soil cosmogenic component of Pepin et al. (1995). The krypton isotopic data of lunar anorthosites 60025.817, 60215.48 and 65315.142 are consistent with a two-component mixture between atmospheric and cosmogenic end-members (Fig. 4), without excluding the possibility that solar Kr also contributed Kr isotopes. As in the cases of He, Ne and Ar, no primordial component of lunar anorthosite noble gases, distinct from the terrestrial atmosphere, can be identified from Kr isotope data.

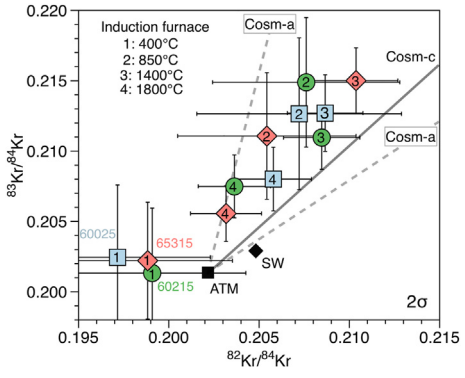

Fig. 4. Kyrpton three-isotope diagram. Error bars are 2σ. Terrestrial atmosphere (ATM) $^{82}Kr/^{84}Kr$: 0.20217, $^{83}Kr/^{84}Kr$: 0.20136 from Basford et al. (1973). Pure cosmogenic (COSMOc) $^{82}Kr/^{84}Kr$: 1.112, $^{83}Kr/^{84}Kr$: 1.276, calculated from Hohenberg et al. (1978) (COSMOa) $^{82}Kr/^{84}Kr$: 2.25 ± 1.44, $^{83}Kr/^{84}Kr$: 3.13 ± 1.95, average lunar bulk soils from Pepin et al. (1995).

4.2. Xenon isotopic data

For all samples and extraction steps, including the high temperature steps, most of the Xe isotope ratios measured in this study are close to the terrestrial atmospheric values (Basford et al., 1973, Table A6 in Appendix A). This confirms the previous interpretations that (i) terrestrial noble gases are present in lunar anorthosite, and (ii) common physical adsorption cannot account for the high temperature required to release this contaminant (Lightner and Marti, 1974; Leich and Niemeyer, 1975; Niemeyer and Leich, 1976).

As expected from the very short exposure ages (Meyer, 2011; Meyer, 2012) of these samples and in agreement with previous studies (Lightner and Marti, 1974; Leich and Niemeyer, 1975), we measured low abundances of cosmogenic isotopes, only revealed by small excesses in $^{124-126}Xe$ isotopes. The heavy Xe isotopes ($^{134,136}Xe$) appear to be depleted relative to the terrestrial atmosphere composition for most of the temperature steps (Fig. 6). The mean deficit in ^{136}Xe ($\delta^{136}Xe = -9.65 \pm 2.91‰$ (2σ), relative to ^{132}Xe and modern atmosphere, Fig. 5) is significant and reproducible.

The barium and lanthanum contents, which are the main target elements for Xe cosmogenic production, are: [Ba] = 9.69 ppm, 10.62 ppm and 5.19 ppm and [La] = 0.39 ppm, <0.2 ppm and 0.29 ppm, for samples 60025.817, 60215.48 and 65315.142, respectively (Table A1 in Appendix A). Cesium and neodymium contents, which could also contribute to the spallation-produced Xe budget (Hohenberg et al. 1981), are: [Ce] = 2.54 ppm, 1.95 ppm and 3.08 ppm and [Nd] = 0.44 ppm, 0.18 ppm and 0.25 ppm, respectively (Table A1 in Appendix A). In considering sample exposure ages from the literature (Meyer, 2011; Meyer, 2012) and the Xe cosmogenic production

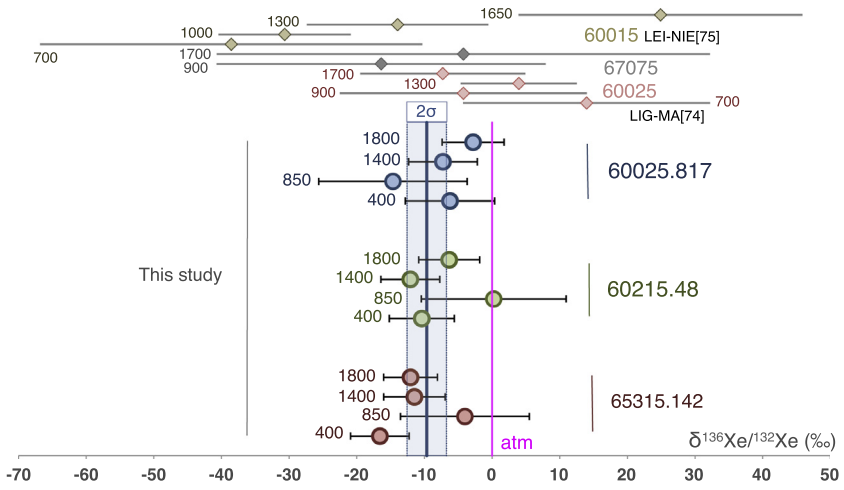

Fig. 5. Deviation of $^{136}Xe/^{132}Xe$ from the terrestrial atmosphere for lunar anorthosites 65315, 60025 and 60215, measured by stepwise heating in an induction oven system. Deviation is expressed with the delta notation ($\delta^{136}Xe/^{132}Xe = \{(^{136}Xe/^{132}Xe_{sample})/(^{136}Xe/^{132}Xe_{atm}) - 1\} \times 1000$). Data from previous studies (Lightner and Marti, 1974; Leich and Niemeyer, 1975) are shown on top. Error bars represent 2σ. The error-weighted mean is indicated by the blue line, and its 2σ error envelope is given by the blue box (MSWD = 0.74). Extraction temperatures are in °C. Mean $^{136}Xe/^{132}Xe$ over our study =0.32622 ± 0.00096 (2σ), ATM: Basford et al. (1973). (For interpretation of the references to colour in this figure legend, the reader is referred to the web version of this article.)

rates from Hohenberg et al. (1978) - based on samples target element concentrations and for a shielding of 2 g/cm^2 - we find that corrections for cosmogenic isotope contributions are negligible for the $^{128–136}Xe$ isotopes (the isotopic composition of the cosmogenic end-member calculated for each sample is given in Appendix A, Table A6). Cosmogenic isotopes account for less than 2% of total ^{126}Xe and less than 0.1% of total $^{129–136}Xe$, which is within analytical error. Estimates of the maximum corrections for spallation contributions (Fig. 6) were performed in assuming that any $^{126}Xe/^{130}Xe$ deviation from the terrestrial atmosphere results from mixing between a pure cosmogenic component and atmospheric Xe (Lightner and Marti, 1974; Leich and Niemeyer, 1975), ^{126}Xe being the most sensitive isotope to cosmogenic contributions. An estimate of the cosmogenic contribution for a given Xe spectrum can then be calculated and propagated to the other isotopes. By knowing (i) the contribution of the cosmogenic component and (ii) the isotopic composition of this end-member (taken as the average lunar isotopic composition of cosmogenic Xe, Pepin et al. (1995), given in Appendix A Table A6), all isotope spectra can be corrected for spallation-produced isotopes (Fig. 6). After correction, ^{134}Xe and ^{136}Xe are thus still depleted, especially in samples 60215 and 65315 (Fig. 7). Production of Xe isotopes by nuclear reactions will contribute, and not deplete, heavy isotopes through spontaneous or induced fission of $^{235,238}U$ and ^{244}Pu, and thus cannot be advocated here. The origin and implications of such deviations from the terrestrial atmosphere composition are discussed in section 6.

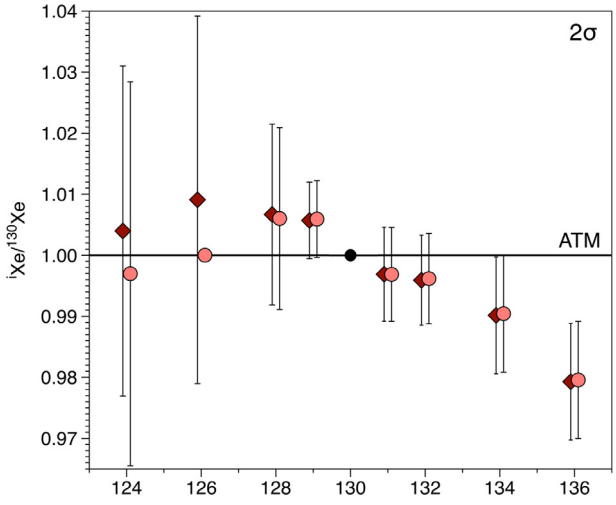

Fig. 6. Xenon isotopic spectra of the lunar anorthosite 65315 400 °C extraction step, non-corrected (diamonds) and corrected (circles) for cosmogenic contribution (see text for explanation of the correction method). Isotope ratios are normalized to the isotopic composition of atmospheric Xenon (ATM: Basford et al. (1973)). Error bars are 2σ.

4.3. Infrared reflectance spectroscopy

We tested the possibility of Xe chemical bonding (chemisorption) on anorthosite using IR-reflectance spectroscopy to characterize the nature and strength of bonding between Xe and anorthosite. While detection of a chemical bond between Xe and anorthosite would have force constants that result in low-frequency far-infrared absorption bands (not available in the present instrumentation), the effect of such bonding on the vibrational frequencies of the functional groups of the anorthosite that are involved should be easily detected. If the interaction between adsorbed Xe and anorthosite is strong enough to modify the strength of bonding between the anorthosite atoms, such as Fe and O, then a shift in the absorbance peak of anorthosite is expected. A shift towards lower wavenumbers could be due to weakening of these bonds as a result

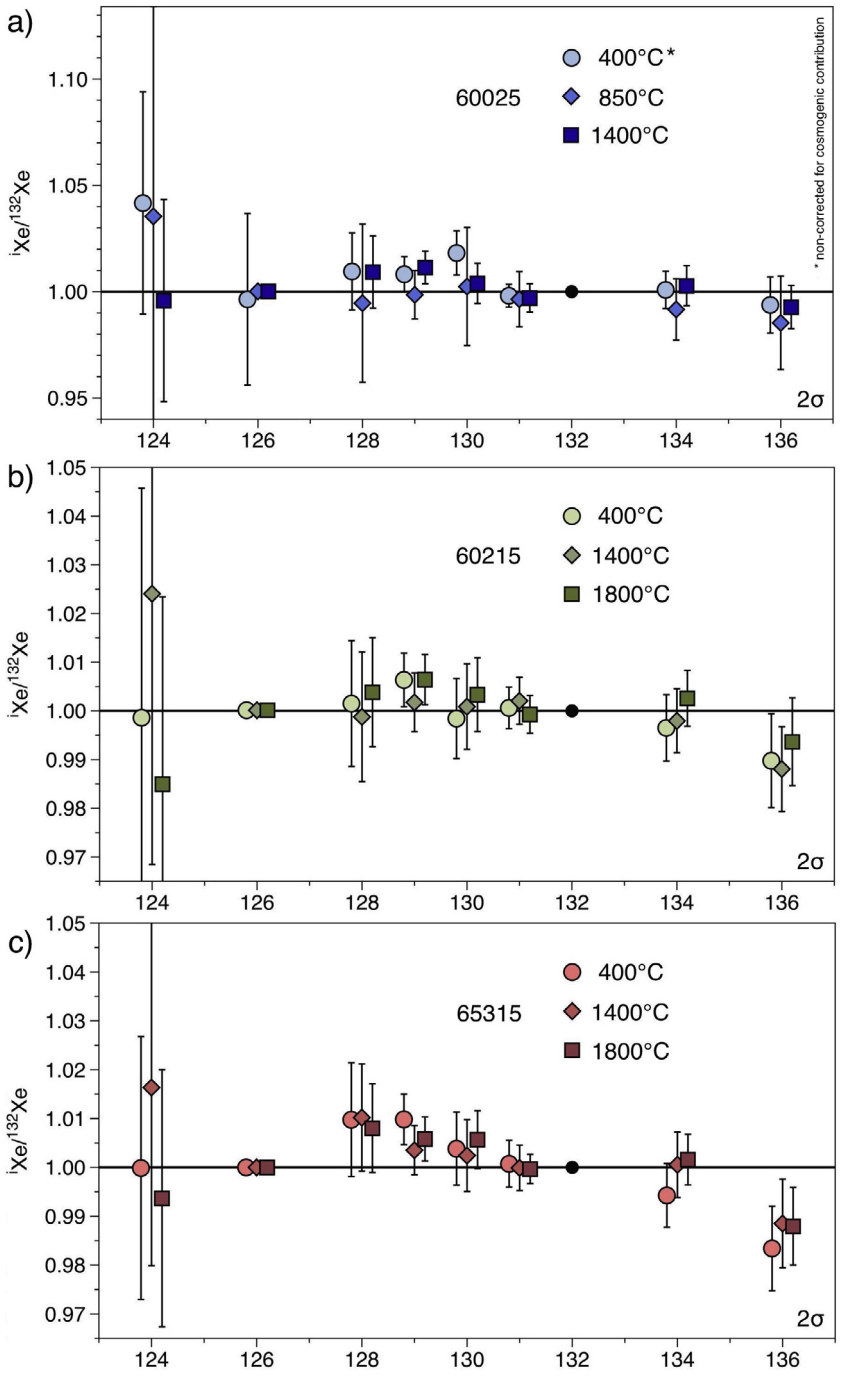

Fig. 7. Xenon isotopic spectra of lunar anorthosites 60025, 60215 and 65315, at 400 °C, 850 °C and 1400 °C for sample 60025, and 400 °C, 1400 °C and 1800 °C for samples 60215 and 65315. All data shown are normalized to the isotopic composition of atmospheric Xe and have been corrected for cosmogenic contribution except the 400 °C extraction step of sample 60025, for which the $^{126}Xe/^{132}Xe$ was lower than the atmospheric ratio, and thus no correction could be made. ATM: Basford et al. (1973). Error bars are 2σ.

of interaction with Xe, which would move the electron density away from the bond. On the other hand, a shift towards the higher wavenumbers would indicate that Xe acts as an electron donor and so strengthens the covalent bond (increased electron density). Thus, any spectral shift observed between the spectra measured before and after exposure to Xe would indicate chemisorption of Xe with the mineral molecules.

Our results support the hypothesis of chemical bonding between Xe and anorthosite. Fig.8a shows a comparison between the anorthositic powder absorbance spectra, before and after 22 hours of exposure to Xe. A significant shift to lower wavenumbers is detected for the 1150 cm^{-1} anorthosite peak after adding Xe to the system (Fig. 8b). Note that another absorption band at 950 cm^{-1} remains unaltered, indicating that bonds responsible for this absorp-

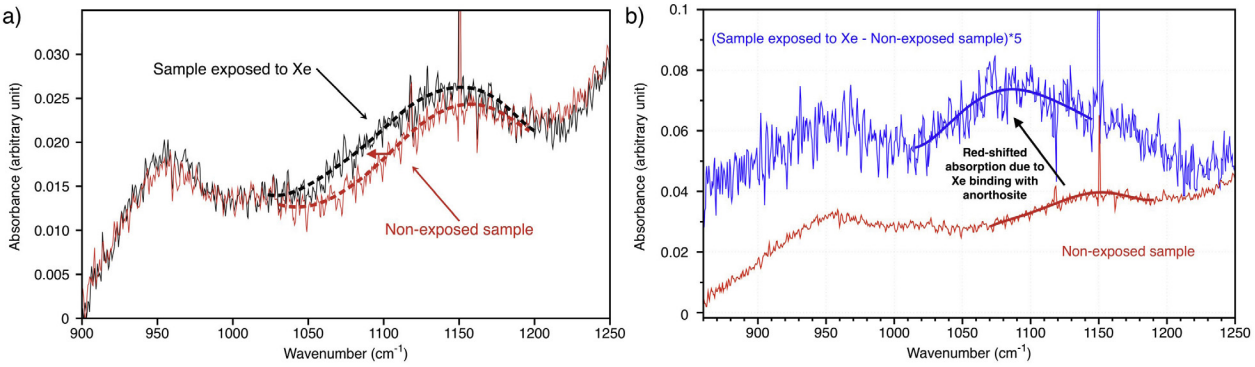

Fig. 8. (a) Absorption spectra of the lunar anorthositic powder, before (in red) and after (in black) exposure to a ~500 mbar pure xenon atmosphere for 22 h. The red arrow indicates a shift toward lower wavenumbers in the absorbance peak at ~1150 cm^{-1} when Xe is added, interpreted as an evidence of Xe chemical bonding to anorthosite. (b) The blue curve shows the magnified (x5) subtraction of the lunar anorthosite absorbance spectrum before addition of Xe (in red) from the absorbance spectrum of the lunar anorthosite exposed to Xe for 22 h (black curve on panel a). While a flat spectrum would indicate no change in the absorbance peaks of lunar anorthosite, the blue curve reveals the occurrence of a shift in the 1150 cm^{-1} lunar anorthosite IR absorbance peak induced by Xe chemisorption. (For interpretation of the references to color in this figure legend, the reader is referred to the web version of this article.)

tion were not accessible for Xe to interact and hence were not affected. This chemical interaction between Xe and the anorthosite could be at the origin of the anomalous adsorption proposed by previous authors (Lightner and Marti, 1974; Leich and Niemeyer, 1975; Niemeyer and Leich, 1976) and thus could explain the origin of the dominant terrestrial Xe component in lunar samples. In this study, small deviations (at the level of a few permil) from the isotopic composition of the terrestrial atmosphere have also been detected. Several explanations can be proposed for the origin of the lunar anorthosite depletion in Xe heavy isotopes and these are discussed in the next section.

5. DISCUSSION

The isotopic compositions of lunar anorthosites, including those analyzed in this study, are very close to that of the terrestrial atmosphere (Eugster, 1986). The trapping of terrestrial Xe is probably due to chemisorption of atmospheric xenon rather than common physical adsorption through Van der Waals bonding. This was suggested by previous trapping experiments that showed evidence for anomalous adsorption of Xe onto lunar anorthosites (Niemeyer and Leich, 1976; Niedermann and Eugster, 1992) and is confirmed here by observation of Xe chemical bonding by IR spectroscopy. However, high precision Xe isotope analyses show that heavy Xe isotopes are often depleted relative to terrestrial atmosphere. Such ^{134,136}Xe depletion could be due to mass-dependent isotope fractionation (MDF), mass-independent isotope fractionation (MIF), and/or contribution of a non-terrestrial Xe component. Note that these processes are not mutually exclusive, thus the extent of each needs careful evaluation. MIF has never before been demonstrated for Xe isotopes, thus, while this does not mean that MIF is impossible, in the absence of experimental/observational evidence for this phenomenon we consider the two other possibilities as more likely explanations.

Straight-line fitting calculations on lunar anorthosite Xe were performed in order to investigate the possibility of a contribution from a MDF component, possibly attributed to MDF terrestrial Xe (Table A7 in Appendix A). As corrections for the cosmogenic contribution assume that the trapped ^{126}Xe/^{130}Xe ratios represent the unfractionated atmospheric value (which would be incorrect if the trapped Xe component actually was MDF atmospheric Xe), straight-line fitting calculations were carried on the non-corrected data by taking into account only the $^{128-136}$Xe/^{132}Xe isotope ratios (which are negligibly affected by the cosmogenic contribution (Fig. 6)). While the probability of MDF is sometimes low (e.g., probability of 0.17 and MSWD of 1.5 for sample 65315 at 1800 °C, with a slope of -0.00199 ± 0.0014 at 2σ), the data consistently show some agreement with MDF (e.g. for sample 65315 at 400 °C, which gives a probability and a MSWD of 0.82 and 0.43, respectively, with a slope of -0.00316 ± 0.001, 2σ). Potentially, MDF of the trapped Xe component could have taken place during the anomalous adsorption of atmospheric Xe onto lunar anorthosites. However, it has been demonstrated experimentally that adsorption of neutral xenon on to solid surfaces does not yield any measurable isotopic fractionation (with a maximum fractionation factor estimated to be $-0.2‰ \pm 0.1‰$ per u, see Marrocchi and Marty (2013) and references therein). Significant isotopic fractionation can only occur when Xe is ionized. In this case, trapping of Xe ions onto solids always results in enrichments in the heavy isotopes relative to the light isotopes (Dziczkaniec et al., 1981; Bernatowicz and Fahey, 1986; Bernatowicz and Podosek, 1986; Bernatowicz and Hagee, 1987; Ponganis et al., 1997; Koscheev et al., 2001; Hohenberg et al., 2002; Huss et al., 2008; Marrocchi et al., 2011; Kuga et al., 2015). Such MDF does not depend on the chemical nature of the solid surface (i.e., organic, glass, metal or mineral), nor on the energetic regime of the ion–solid interaction (i.e., adsorption for $E \sim 50$ eV, sputtering for $50 < E < 500$ eV and implantation for

$E > 500$ eV) (Marrocchi et al., 2011). Thus, the fact that the heavy, and not the light, Xe isotopes are depleted in lunar anorthosite is unexpected because trapping in solids would favor the heavy isotopes, which is inconsistent with the Xe depletion in heavy isotopes reported here. Even though our data cannot rule out MDF, a MDF process that would deplete, and not enrich, the heavy Xe isotopes relative to the light ones would need to be identified. In the absence of evidence for such a process, we therefore discuss next the possibility of mixing between anomalously adsorbed modern atmospheric Xe and a trapped non-atmospheric component.

The putative non-atmospheric Xe component trapped in lunar anorthosite could have been inherited from ancient terrestrial atmosphere implanted on the lunar surface (the so-called Earth's wind, Ozima et al., 2005). Based on analysis of Xe trapped in Archean rocks, Pujol et al. (2011) proposed that the terrestrial atmosphere Xe evolved progressively from a primitive component, chondritic or solar, by MDF and that the present-day enrichment of heavy Xe isotopes in the atmosphere relative to cosmochemical end-members was not yet complete ≥3 Gyr ago. Recently, Avice et al. (2017), through high precision analyses of noble gases trapped in fluid inclusions of Archean quartz (~3.3 Ga, Barberton, South Africa), determined that the primordial Xe component of the Earth's atmosphere is distinct from solar or chondritic Xe but similar to a theoretical component labeled U-Xe (Fig. 9). According to Pepin et al. (1995), terrestrial atmospheric Xe evolved from this theoretical primitive component (identical to the solar composition for all Xe isotopes but depleted in $^{134–136}$Xe) by MDF and addition of fissiogenic ($^{131–136}$Xe) and radiogenic (^{129}Xe) isotopes. The Xe mass fractionation could have evolved over 2 Gyr following Earth's formation (Pujol et al., 2011), and thus the modern atmosphere-like composition of the $^{124–132}$Xe isotopes might have only been reached after this interval of time. Fissiogenic Xe isotopes (mainly $^{134–136}$Xe) have been added to the Earth's atmospheric Xe inventory by spontaneous fission of ^{244}Pu and ^{238}U throughout its history. The Xe isotope composition of lunar anorthosites could therefore represent an ancient atmospheric Xe component that had already reached a close-to-modern Xe composition but that had not received the full fissiogenic contribution of heavy Xe isotopes observed in the modern terrestrial atmosphere. This would imply implantation of terrestrial atmosphere isotopes into lunar soils, as proposed by Ozima et al. (2005) for the origin of lunar nitrogen and light noble gases. Recent observations from the Japanese spacecraft Kaguya indicate that when the Moon is in Earth's plasma sheet today, modern terrestrial oxygen ions can be transported to the Moon's surface and implanted into the lunar regolith (Terada et al., 2017). Thus, ancient terrestrial atmosphere gases could similarly be preserved on the present-day lunar surface. However, the low exposure ages of lunar anorthosites 60025, 60215 and 65315, related to their recent excavation by the South Ray crater event 2 Myr ago (Eugster, 1999), do not support their exposure in the distant past. This hypothesis is also inconsistent with the fact that we do not observe implanted terrestrial nitrogen enriched in ^{15}N, as suggested by Ozima et al. (2005).

The occurrence of the U-Xe signature in the primitive terrestrial atmosphere (Avice et al., 2017) is at odds with the chondritic signature of terrestrial mantle Xe (Caracausi et al., 2016). Such a dichotomy between Earth's mantle and atmosphere leaves little space for a genetic link between the two reservoirs and an exotic origin of the progenitor of atmospheric Xe has often been advocated (e.g. Swindle and Kring, 1997; Morbidelli et al., 2000; Dauphas, 2003; Raymond et al., 2004; Marty and Meibom, 2007; Marty, 2012; Albarède et al., 2013; Marty et al., 2016). Potential carriers of this primordial component include volatile-rich bodies originating from large heliocentric distances in the outer solar system. Importantly, the contribution of cometary volatiles to the Earth's inventory, minor for water (≤1%), carbon (≤1%) and nitro-

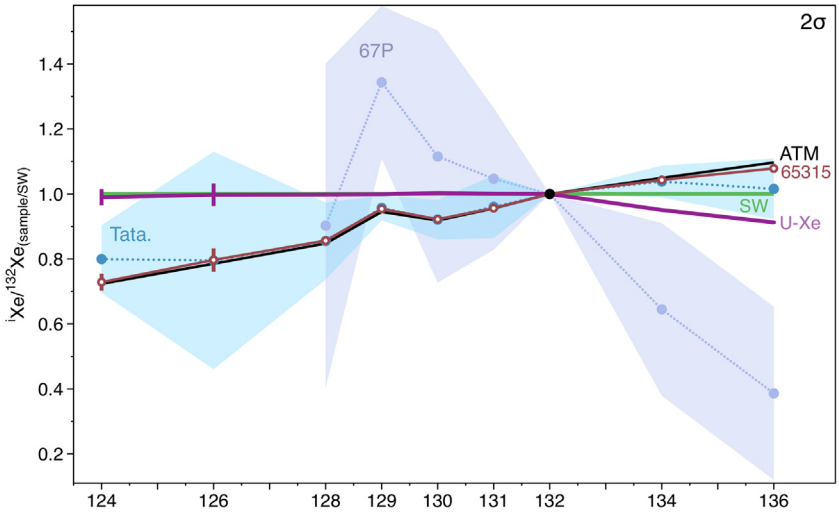

Fig. 9. Xenon isotopic spectra of lunar anorthosite 65315.142, 400 °C, normalized to solar wind (SW) (Meshik et al., 2014) and compared to terrestrial atmospheric Xe (Basford et al., 1973), U-Xe (Pepin and Porcelli, 2002), Xe isotope composition of comet 67P/Churyumov-Gerasimenko (Marty et al., 2017) and Tatahouine data for extraction at 600 °C (Michel and Eugster, 1994). Error bars are 2σ.

gen species ($\leq$ a few%), would have been significant for noble gases (Marty et al., 2016). While traces of such bombardment episodes are seen on the present-day surface of the Moon (Ong et al., 2010; Bogard, 2011), no noble gas components originating from the volatile-rich bodies that participated in building the Earth's atmosphere inventory have ever been detected on the Moon. Recently, the Rosetta Orbiter Spectrometer for Ion and Neutral Analysis (ROSINA) onboard the Rosetta spacecraft analyzed the xenon isotopic composition of comet 67P/Churyumov-Gerasimenko (Fig. 9, Marty et al., 2017). This unique data of the isotopic composition of Xe in a comet (here after labeled 67P-Xe) matches that of the U-Xe component (Pepin, 1994) and demonstrates that cometary Xe contributes to the terrestrial atmosphere Xe inventory (Marty et al., 2017). Thus, the detection of heavy xenon isotope deficits and slight mass fractionation patterns across $^{128–136}$Xe isotopes in lunar anorthosites could be attributed to remnants of a U-Xe-like component that was brought to the Moon during the very last stages of terrestrial accretion, before being subsequently mixed with anomalously adsorbed modern atmospheric Xe. This hypothesis is in line with the Xe isotopic spectra measured by Michel and Eugster (1994) in the Tatahouine diogenite. In the 1000 °C and 1200 °C extraction steps, they measured Xe isotopic compositions similar to that of U-Xe proposed by Pepin and Phinney (1978). In the 600 °C, 800 °C and 1600 °C temperature steps, the Xe isotopic spectra showed intermediate signatures between terrestrial atmosphere and U-Xe. Even if subsequent experiments did not reproduce their results (Busemann and Eugster, 2002), at 600 °C and 800 °C, the Xe isotope compositions were comparable to those reported here for lunar anorthosites (Fig. 9).

Alternatively, the apparent deficit in heavy Xe isotopes could be the result of a contribution of SW-Xe. Niedermann and Eugster (1992) also measured deficits in heavy Xe isotopes in sample 65315 compared to terrestrial atmosphere when normalized to solar wind. They proposed that the measured composition was the result of mixing between atmospheric and solar wind components. In light of the Ne and Ar isotope measurements, the presence of a solar Xe component in samples 60025 and 60215 cannot be dismissed. This SW component could possibly have been derived from contamination by dust previously exposed to the solar wind that polluted the samples during their preparation. To test this possibility, we estimated the contribution from solar ^{20}Ne and ^{36}Ar and extrapolated it to Xe based on the ^{132}Xe/^{20}Ne and ^{132}Xe/^{36}Ar ratios of the solar wind [Grimberg et al., 2008; Vogel et al., 2011]. For neon, we estimated the SW contribution by projecting the data on the ATM-SW line, following a straight line drawn through the cosmogenic end-member and the data points. The SW contribution was then derived as:

$$\text{SW-Ne}\ (\%) = \frac{^{20}\text{Ne}/^{22}\text{Ne}_{\text{projection}} - ^{20}\text{Ne}/^{22}\text{Ne}_{\text{ATM}}}{^{20}\text{Ne}/^{22}\text{Ne}_{\text{SW}} - ^{20}\text{Ne}/^{22}\text{Ne}_{\text{ATM}}} \quad (3)$$

The estimated SW contribution was applied to the total amount of ^{20}Ne extracted from the sample, thus assuming that any variation in the ^{20}Ne/^{22}Ne ratio would be caused by a change in the amount of ^{20}Ne (no input or loss of ^{22}Ne). For Ar, the data corrected for cosmogenic ^{36}Ar and with ^{40}Ar/^{36}Ar lower than the atmospheric ratio were projected onto the ATM-SW line and the SW contribution was estimated in the same way as for neon. The estimated contribution of the SW was applied to the total amount of ^{36}Ar extracted from the sample, thus assuming that any variation in the ^{40}Ar/^{36}Ar ratio would be caused by a change in the amount of ^{36}Ar (no input or loss of ^{40}Ar). For Ar (sample 60215 at 850 °C and 1400 °C), the derived amounts of SW-Xe (mol/g) were compared to the actual amounts of ^{132}Xe (mol/g) extracted during the respective steps. For both extraction steps, we find that the SW-Xe would contribute less than 0.7% of the extracted ^{132}Xe. For Ne, as we could not compare the Ne and Xe data based on a common extraction step, we derived amounts of SW-^{132}Xe (mol/g) for samples 60025 and 60215 and compared them to the total amounts of ^{132}Xe (mol/g) extracted for each samples. By doing so, we find that the derived solar contribution would not exceed 0.003% of the extracted ^{132}Xe. The contributions of SW-Xe calculated using Ne data are much lower than those estimated from Ar data. This difference could be due to the fact that the $(\text{Ne/Ar})_{\text{SW}}$ ratios in lunar samples are much lower than the values in the solar wind proper, especially for plagioclase-rich lunar highlands samples, because plagioclase is poorly retentive for SW-Ne (and even less so for SW-He, (Signer et al. 1977)). If the ^{132}Xe/^{20}Ne ratio of the Apollo 16 soil [Bogard et al., 1973] is used instead of that of the pure SW (appropriate here since a SW-Xe "contamination" of the samples would likely be by fine lunar dust from the Apollo 16 site), we find that the derived solar contribution would not exceed 0.3% of the extracted ^{132}Xe. When based on the ^{132}Xe/^{36}Ar ratio of the Apollo 16 soil [Bogard et al., 1973], the estimated solar contributions are lower than 0.9% of the extracted ^{132}Xe. Note that a possible reason for the lower Ne-derived SW-Xe contribution would be that the laser might not have quantitatively extracted Ne, as suggested by the lower exposure ages obtained in this study from ^{21}Ne (Table 1). However, even 1% of SW-Xe addition, as obtained here from Ar data, would only reduce ^{136}Xe/^{132}Xe by 0.9‰, i.e. about one order of magnitude less than the ^{136}Xe/^{132}Xe deviation reported here. This argues for a negligibly small contribution of SW-Xe in our samples. Note that for sample 65315, which exhibits the largest deviations relative to the isotopic composition of the terrestrial atmospheric Xe (Fig. 7), no contribution of SW gases is detected from He-Ne-Ar-Kr-N_2 data.

The U-Xe and SW-Xe signatures are isotopically close (identical for all Xe isotopes but $^{134–136}$Xe, which are depleted in U-Xe) (Fig. 9). In order to assess the statistical likeliness of contributions from SW-Xe, U-Xe, or 67P-Xe components in lunar anorthosites, we performed Monte-Carlo simulations involving mixing atmospheric Xe with (i) pure SW-Xe, (ii) pure U-Xe, or (iii) pure 67P-Xe, respectively. The method is detailed below for mixing calculations of SW-Xe vs. U-Xe (Fig. 10), the same approach being thereafter carried for contribution of SW-Xe vs. 67P-Xe (for which $^{128–136}$Xe isotopes only could be used, Fig. 11). For each run of Monte Carlo error-propagation simulations, a Gaussian distribution was assumed for the

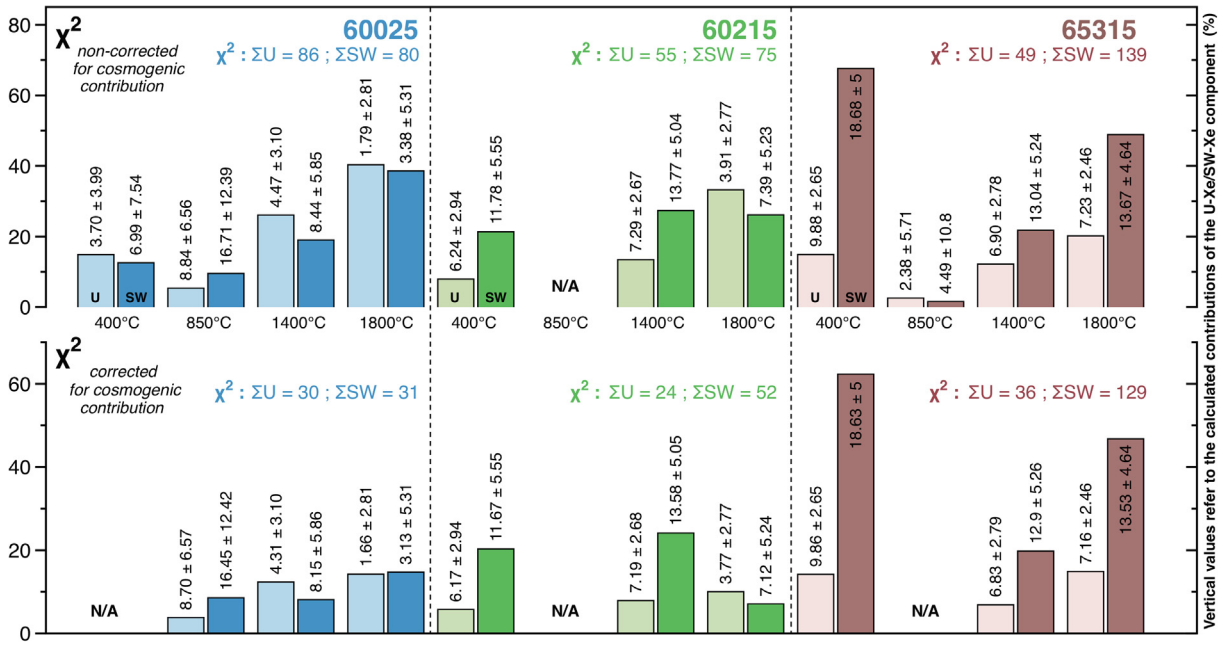

Fig. 10. Comparison of the χ^2 values calculated when comparing the Xe isotopic data measured in lunar anorthosites and the theoretical Xe isotopic compositions computed from mixing between ATM-Xe and either U-Xe or SW-Xe. The upper part refers to mixing calculations aiming at reproducing the data non-corrected for a cosmogenic contribution, while the lower part reports calculations made with the corrected data. Comparisons of χ^2 values calculated with the U-Xe and SW-Xe compositions are given for each temperature step, with the respective contributions of the U-Xe/SW-Xe components marked vertically (%). For each sample, ΣU and ΣSW respectively are the sums of the χ^2 values integrated over the four temperature steps. No data is given for sample 60215 at 850 °C as the measured $^{136}Xe/^{132}Xe$ ratio was only slightly higher than the atmospheric value and thus a mixing calculation could not be performed. Likewise, no correction for a cosmogenic contribution could be made for sample 60025 at 400 °C and sample 65315 at 850 °C as the $^{126}Xe/^{132}Xe$ ratios detected were lower than the atmospheric value.

$^{136}Xe/^{132}Xe$ ratios of the atmospheric Xe (Basford et al., 1973), U-Xe (Pepin and Porcelli, 2002) and lunar anorthosite Xe and a random function permitted to pick one value for each component. The proportion of U-Xe versus Atm-Xe was computed as:

$$\frac{^{136}Xe_{U\text{-}Xe}}{^{136}Xe_{atm}} = \frac{\left(\frac{^{136}Xe}{^{132}Xe}\right)_{atm} - \left(\frac{^{136}Xe}{^{132}Xe}\right)_{mes}}{\left(\frac{^{136}Xe}{^{132}Xe}\right)_{mes} - \left(\frac{^{136}Xe}{^{132}Xe}\right)_{U\text{-}Xe}} \quad (4)$$

where $(^{136}Xe/^{132}Xe)_{atm}$, $(^{136}Xe/^{132}Xe)_{U\text{-}Xe}$, $(^{136}Xe/^{132}Xe)_{mes}$ are the $^{136}Xe/^{132}Xe$ ratios randomly picked in the 1σ distribution of atmospheric Xe, U-Xe and lunar anorthosite Xe components, respectively. The proportions of each component (U-Xe vs. Atm-Xe in the given example) and their associated errors were calculated as the mean and the standard deviation of the 10^6 calculated proportions, respectively. A theoretical Xe isotopic spectrum with related errors were then computed for each temperature step extraction by propagating these proportions of U-Xe (or SW-Xe) toward the lighter isotopes $^{124-134}Xe$ using Monte Carlo error-propagation simulations (10^6 runs). Chi-squared values were then derived in order to evaluate the consistency between the theoretical and the measured isotopic compositions:

$$\chi^2 = \sum_i \frac{\left(\left(\frac{^iXe}{^{132}Xe}\right)_{mes} - \left(\frac{^iXe}{^{132}Xe}\right)_{theo}\right)^2}{\sigma_{mes}(i)^2} \quad (5)$$

where $(^iXe/^{132}Xe)_{mes}$ and $(^iXe/^{132}Xe)_{theo}$ are the $^iXe/^{132}Xe$ ratios measured for lunar anorthosites extraction steps and derived from Monte Carlo simulations, respectively, and $\sigma_{mes}(i)$ is the error in the measured $(^iXe/^{132}Xe)$ ratio at the 1σ level. Thus, a good fit between theoretical isotopic compositions determined from mixing calculations and isotopic measurements will correspond to low χ^2 values, whereas a poor fit expressing high discrepancies between theory and measurements will lead to high χ^2 values. In order to avoid any bias induced by the correction for a cosmogenic contribution, simulations were run for both the non-corrected and corrected datasets.

For the non-corrected data, summing the χ^2 values over the four temperature steps for each sample leads to χ^2 totals of 86, 55 and 49 (using U-Xe) and 80, 75 and 139 (using SW-Xe) for samples 60025, 60215 and 65315, respectively (Fig. 10). In agreement with the very small amplitudes of deviation relative to the terrestrial atmospheric composition for sample 60025 (Fig. 7), the calculated contributions of U-Xe/SW-Xe have large errors (*vertical values,* Fig. 10) and no clear discrimination between a contribution from one of these two components can be detected. For sample 60215, mixing calculations involving the addition of SW-Xe result in sums of χ^2 values that are 40% and 100% higher than those obtained using U-Xe for non-corrected and corrected data, respectively. For sample 65315, which shows the largest deviations relative to the terrestrial atmospheric

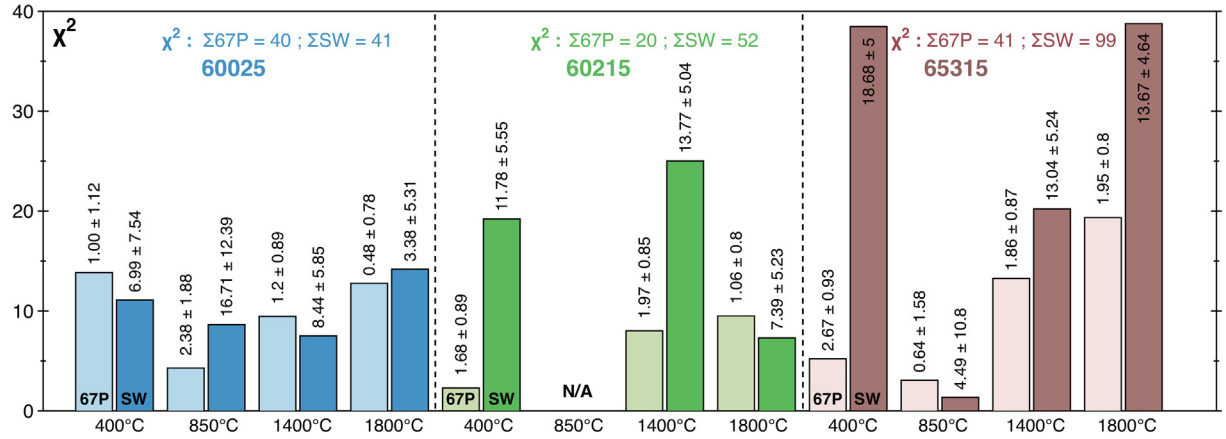

Fig. 11. Comparison of the χ^2 values calculated when comparing the $^{128-136}$Xe isotopes data measured in lunar anorthosites and the theoretical Xe isotopic compositions computed from mixing between ATM-Xe and either 67P-Xe or SW-Xe. Comparisons of χ^2 values calculated with the 67P-Xe and SW-Xe compositions are given for each temperature step, with the respective contributions of the 67P-Xe/SW-Xe components marked vertically (%). For each sample, Σ67P and ΣSW respectively are the sums of the χ^2 values integrated over the four temperature steps. No data is given for sample 60215 at 850 °C as the measured ^{136}Xe/^{132}Xe ratio was only slightly higher than the atmospheric value and thus a mixing calculation could not be performed.

composition (Fig. 7), the discrimination between contributions from SW-Xe or U-Xe components is clear, with much lower χ^2 values calculated for mixing calculations involving the contribution of U-Xe (Fig. 10). In detail, mixing calculations involving the addition of SW-Xe result in sums of χ^2 values that are 180% and 250% higher than those obtained with U-Xe for non-corrected and corrected data, respectively. The SW-Xe contributions calculated to account for the ^{136}Xe deficits are so high that the associated theoretical ratios for the lighter isotopes are overestimated compared to the measured data, resulting in higher χ^2 values. From there, any correction from cosmogenic contribution tends to lower the isotopic ratios of the lighter isotopes and to increase the discrepancies between the χ^2 values calculated with U-Xe and SW-Xe (Fig. 10). Thus, when mixed with ATM-Xe, the U-Xe component is clearly a better candidate than SW-Xe to account for the trapped Xe component measure in lunar anorthosites 60215 and 65315. The maximum estimated contribution of the U-Xe component reaches 9.8 ± 2.6% for the 400 °C extraction step of sample 65315.

The same exercise has been carried out with the 67P-Xe signature in order to compare the statistical likeliness of a contribution from either cometary Xe or SW-Xe. As ^{124,126}Xe isotopes could not be measured for 67P-Xe (Marty et al., 2017), Monte Carlo simulations and χ^2 tests were performed for the data not corrected for a cosmogenic contribution, by considering the $^{128-136}$Xe isotopes only. As observed for the U-Xe component, a contribution from 67P-Xe is unclear for sample 60025, but likely for samples 60215 and 65315 (Fig. 11). Importantly, mixing calculations involving the addition of SW-Xe result in sums of χ^2 values that are about 250% higher than those obtained with 67P-Xe for samples 60215 and 65315 (Fig. 11). The estimated contribution of the 67P-Xe component for the 400 °C extraction step of sample 65315 reaches 2.67 ± 0.93% (Fig. 11).

Importantly, the detection of cometary Xe in samples 60215 and (more reliably) 65315 could represent the first evidence for contribution from volatile-rich bodies at the surface of the Moon. While the 67P-Xe signature refers to a pure cometary end-member, the U-Xe signature corresponds to 22 ± 5% cometary xenon, in addition to chondritic (or solar) xenon (Marty et al., 2017). Thus, the U-Xe signature would correspond to a "less pure" cometary end-member than 67P-Xe. The fact that a contribution from a U-Xe like component is a possibility here leaves space for a contribution of chondritic and/or solar xenon, in addition to pure cometary Xe. Note that the two-stage ^{40}Ar/^{39}Ar release curve identified by Stettler et al. (1974) is consistent with at least two major metamorphic episodes (3–4 Gyr ago and ~2 Gyr ago, respectively) experienced by sample 65315. One or more of these metamorphic events could be directly related to high-energy impacts of volatile-rich bodies on the Moon's surface. Such impacts would generate high-energy sites (Garrison et al., 1987; Hohenberg et al., 2002; Marrocchi et al., 2011) and new active surfaces on lunar rocks, where the anomalous adsorption of Xe from the volatile cloud of the gas-rich impactor could occur (in agreement with high ^{132}Xe/^{36}Ar ratios measured for sample 65315 especially, relative to the mean ^{132}Xe/^{36}Ar ratio reported for Apollo sites (Wieler, 2002), see Fig. C2 in Appendix C). This material would have been rapidly buried under other ejecta and shielded from cosmogenic rays until the South Ray cratering event (Eugster, 1999). Alternatively, a volume-distributed incorporation of cometary gases within the lunar crust minerals could have taken place during the episodes of Lunar Magma Ocean, before the LHB 4.0–3.8 Gry ago (Hartmann et al., 2002; Morbidelli et al., 2012; Bottke et al., 2012).

6. CONCLUSION

Helium, neon, argon and krypton isotope data of lunar anorthosites 60025.817, 60215.48 and 65315.142 are consistent with a three end-member mixture of atmospheric,

cosmogenic and solar wind-like components, the latter suggested by Ne and Ar isotopic variations. As seen in previous studies (Lightner and Marti, 1974; Leich and Niemeyer, 1975), Xe isotope data are dominated by a terrestrial-like component extracted at different temperatures up to 1800 °C (along with cosmogenic isotopes) and previously attributed to "anomalous adsorption" of terrestrial Xe. In order to understand the unexpected occurrence of this atmospheric component at high temperature, we performed IR reflectance spectroscopy measurements on lunar anorthositic powder, before and after exposure to a pure-Xe atmosphere, and detected a shift in the infrared absorbance peaks of the anorthosite when exposed to Xe. This observation accounts for the chemisorption of terrestrial atmospheric Xe onto lunar samples, probably during terrestrial storage and handling. However, the high precision isotopic measurements of lunar anorthosites reveal reproducible deficits in the heavy xenon isotopes ($^{134–136}$Xe), with a δ^{136}Xe of $-9.65 \pm 2.91‰$ (2σ), relative to ^{132}Xe and modern atmosphere. Although we cannot dismiss the possibility of mass-dependent fractionation of Xe isotopes during terrestrial contamination, a process that would deplete, and not enrich, the heavy Xe isotopes needs to be identified. Alternatively, this signature could represent mixing between atmospheric Xe and a trapped component depleted in heavy Xe isotopes (enriched in light Xe isotopes). A contribution from SW-Xe is a possibility, but estimated SW-Xe concentrations based on estimated SW-Ne and SW-Ar concentrations and elemental ratios Ne/Ar/Xe in the solar wind (or in the Apollo 16 soil) show that such contribution would be negligibly small. In addition, Monte-Carlo simulations of atmospheric Xe mixing with pure SW-Xe or U-Xe/67P-Xe suggest that this additional component is more likely related to U-Xe, the precursor of atmospheric Xe (Avice et al., 2017). Interestingly, this additional component could be attributed to cometary xenon (Marty et al., 2017), which would have been brought to the Moon's surface by the volatile-rich bodies that participated in building the Earth's atmosphere inventory during late veneer episodes. A promising avenue for lunar research will be to return samples that have been efficiently isolated from the terrestrial environment.

ACKNOWLEDGEMENTS

Evelyn Füri, Laurent Zimmermann and Yves Marrocchi are acknowledged for participating into fruitful discussions. We are grateful to NASA and CAPTEM for allocation of these precious samples. We thank Rainer Wieler and two anonymous reviewers for their detailed and constructive reviews. This study was supported by the European Research Council (grants no. 267255 and 695618). Part of this work was supported by funding from JPL's DRDF and R&TD funding for infrastructure of the "Ice Spectroscopy Laboratory" at JPL and by NASA funding through the Planetary Atmospheres and Cassini Data Analysis Programs (PI - M. S. Gudipati) and was carried out at the Jet Propulsion Laboratory, California Institute of Technology, under a contract with the National Aeronautics and Space Administration. This is CRPG-CNRS contribution #2521.

APPENDIX A. SUPPLEMENTARY MATERIAL

Supplementary data associated with this article can be found, in the online version, at http://dx.doi.org/10.1016/j.gca.2017.08.041.

REFERENCES

Albarède F., Ballhaus C., Blichert-Toft J., Lee C. T., Marty B., Moynier F. and Yin Q. Z. (2013) Asteroidal impacts and the origin of terrestrial and lunar volatiles. *Icarus* **222**(1), 44–52.

Armytage R. M. G., Georg R. B., Williams H. M. and Halliday A. N. (2012) Silicon isotopes in lunar rocks: Implications for the Moon's formation and the early history of the Earth. *Geochim. Cosmochim. Acta* **77**, 504–514.

Arvidson R., Crozaz G., Drozd R. J., Hohenberg C. M. and Morgan C. J. (1975) Cosmic ray exposure ages of features and events at the Apollo landing sites. *The Moon* **13**, 259–276.

Avice G., Marty B. and Burgess R. (2017) The origin and degassing history of the Earth's Atmosphere Revealed by Archean Xenon. *Nat. Commun.* **8**. https://doi.org/10.1038/ncomms15455.

Basford J. R., Dragon J. C., Pepin R. O., Coscio, Jr., M. R. and Murthy V. R. (1973) Krypton and xenon in lunar fines. In *Proc. Lunar Planet. Sci. Conf*, vol. 4, p. 1915. Proc. Lunar Planet. Sci. Conf.

Bernatowicz T. J. and Fahey A. J. (1986) Xe isotopic fractionation in a cathodeless glow discharge. *Geochim. Cosmochim. Acta* **50**, 445–452.

Bernatowicz T. J. and Hagee B. E. (1987) Isotopic fractionation of Kr and Xe implanted in solids at very low energies. *Geochim. Cosmochim. Acta* **51**, 1599–1611.

Bernatowicz T. J. and Podosek F. A. (1986) Adsorption and isotopic fractionation of Xe. *Geochim. Cosmochim. Acta* **50**, 1503–1507.

Bogard D. D. (2011) K-Ar ages of meteorites: Clues to parent-body thermal histories. *Chemie der Erde-Geochemistry* **71**(3), 207–226.

Bogard D. D., Nyquist L. E., Hirsch W. C. and Moore D. R. (1973) Trapped solar and cosmogenic noble gas abundances in Apollo 15 and 16 deep drill samples. *Earth Planet. Sci. Lett.* **21**(1), 52–69.

Borg L. E., Connelly J. N., Boyet M. and Carlson R. W. (2011) Chronological evidence that the Moon is either young or did not have a global magma ocean. *Nature* **477**(7362), 70–72.

Bottke W. F., Vokrouhlický D., Minton D., Nesvorný D., Morbidelli A., Brasser R., Simonson Bruc and Levison H. F. (2012) An Archaean heavy bombardment from a destabilized extension of the asteroid belt. *Nature* **485**(7396), 78–81.

Busemann H. and Eugster O. (2002) The trapped noble gas component in achondrites. *Meteorit. Planet. Sci.* **37**(12), 1865–1891.

Canup R. M. and Esposito L. W. (1996) Accretion of the Moon from an impact-generated disk. *Icarus* **119**, 427–446.

Canup R. M. (2004a) Formation of the Moon. *Ann. Revs. Astron. Astrophy.* **42**, 441–475.

Canup R. M. (2004b) Simulations of a late lunar forming impact. *Icarus* **168**, 433–456.

Canup R. M. (2013) Lunar conspiracies. *Nature* **504**, 27–29.

Canup R. M., Barr A. C. and Crawford D. A. (2013) Lunar-forming impacts: high-resolution SPH and AMR-CTH simulations. *Icarus* **222**(1), 200–219.

Caracausi A., Avice G., Burnard P. G., Füri E. and Marty B. (2016) Chondritic xenon in the Earth's mantle. *Nature* **533**(7601), 82–85.

Clark R. N., King T. V., Klejwa M., Swayze G. A. and Vergo N. (1990) High spectral resolution reflectance spectroscopy of minerals. *J. Geophys. Res.: Solid Earth* **95**(B8), 12653–12680.

Ćuk M. and Stewart S. T. (2012) Making the Moon from a fast-spinning Earth: a giant impact followed by resonant despinning. *Science* **338**(6110), 1047–1052.

Dauphas N. (2003) The dual origin of the terrestrial atmosphere. *Icarus* **165**(2), 326–339.

Dauphas N., Burkhardt C., Warren P. H. and Fang-Zhen T. (2014) Geochemical arguments for an Earth-like Moon-forming impactor. *Phil. Trans. R. Soc. Lond.* **372**(2024), 20130244.

Drozd R. J., Hohenberg C. M., Morgan C. J., Podosek F. A. and Wroge M. L. (1977) Cosmic-ray exposure history at Taurus-Littrow. In *Proc. Lunar Planet. Sci. Conf*, vol. 8, pp. 3027–3043. Proc. Lunar Planet. Sci. Conf.

Dziczkaniec M., Lumpkin G., Donahue G. and Chang S. (1981) Plasma synthesis of carbonaceous material with noble gas tracers. In *Lunar Planet. Sci. Conf*, vol. 12, pp. 246–248. Lunar Planet. Sci. Conf.

Eberhardt P., Eugster O., Geiss J., Graf H., Grögler N., Morgeli M. and Stettler A. (1975) 81 Kr-Kr exposure ages of some Apollo 14, Apollo 16 and Apollo 17 rocks. *Lunar Sci.* **VI**, 233–235.

Elliott T. and Stewart S. T. (2013) Planetary science: Shadows cast on Moon's origin. *Nature* **504**(7478), 90–91.

Eugster O. (1986) Noble gases in grain size fractions of lunar anorthosite 60018: trapped xenon isotopically similar to terrestrial atmospheric xenon. In *Lunar Planet. Sci. Conf*, vol. 17, pp. 212–213. Lunar Planet. Sci. Conf.

Eugster O. (1999) Chronology of dimict breccias and the age of South Ray crater at the Apollo 16 site. *Meteorit. Planet. Sci.* **34**, 385–391.

Eugster O., Eberhardt P., Geiss J., Grogler N., Jungck M., Meier F., Morgell M. and Niederer F. (1984) Cosmic ray exposure histories of Apollo 14, Apollo 15 and Apollo 16 rocks. *J. Geophys. Res.* **89**, B498–B512.

Füri E., Barry P. H., Taylor L. A. and Marty B. (2015) Indigenous nitrogen in the Moon: Constraints from coupled nitrogen–noble gas analyses of mare basalts. *Earth Planet. Sci. Lett.* **431**, 195–205.

Ganapathy R. and Anders E. (1974) Bulk compositions of the Moon and Earth, estimated from meteorites. In *Proc. Lunar Planet. Sci. Conf*, vol. 5, pp. 1181–1206. Proc. Lunar Planet. Sci. Conf.

Garrison D. H., Olinger C. T., Hohenberg C. M. and Goswami J. N. (1987) Surface-correlated noble gases from grain-size separates of Kapoeta. *Meteoritics* **22**, 382.

Genda H. and Abe Y. (2005) Enhanced atmospheric loss on protoplanets at the giant impact phase in the presence of oceans. *Nature* **433**, 842–844.

Gopalan K. and Rao M. N. (1976) Solar cosmic ray effects in heavy noble gases of lunar soils and breccias. *Lunar Sci.* **VII**, 316–318.

Grimberg A., Baur H., Bühler F., Bochsler P. and Wieler R. (2008) Solar wind helium, neon, and argon isotopic and elemental composition: data from the metallic glass flown on NASA's Genesis mission. *Geochim. Cosmochim. Acta* **72**(2), 626–645.

Hartmann W. K. and Davis D. R. (1975) Satellite-sized planetisimals and lunar origin. *Icarus* **24**, 504–505.

Hartmann W. K., Ryder G., Dones L. and Grinspoon D. (2002) The time-dependent intense bombardment of the primordial Earth/Moon system. In *Origin of the Earth and Moon* (eds. R. M. Canup and K. Righter). Univ. Arizona Press, pp. 493–512.

Hashizume K. and Marty B. (2004) Nitrogen isotopic analyses at the sub-picomole level using an ultra-low blank laser extraction technique. In *Handbook of Stable Isotope Analytical Techniques*, vol. 1, pp. 361–375. Handbook of Stable Isotope Analytical Techniques.

Heber V. S., Wieler R., Baur H., Olinger C., Friedmann T. A. and Burnett D. S. (2009) Noble gas composition of the solar wind as collected by the Genesis mission. *Geochim. Cosmochim. Acta* **73**, 7414–7432.

Hiesinger H. and Head J. W. (2006) New views of lunar geoscience: An introduction and overview. In *New Views of the Moon, Reviews in Mineralogy and Geochemistry* (eds. B. Jolliff and M. Wiezcorek), pp. 1–81.

Hobza P. and Havlas Z. (2000) Blue-shifting hydrogen bonds. *Chem. Rev.* **100**(11), 4253–4264.

Hoffmann F. M. (1983) Infrared reflection-absorption spectroscopy of adsorbed molecules. *Surf. Sci. Rep.* **3**(2–3), 107109–107192.

Hohenberg C. M., Podosek F. A., Shirck J. R., Marti K. and Reedy R. C. (1978) Comparisons between observed and predicted cosmogenic noble gases in lunar samples. In *Proc. Lunar Planet. Sci. Conf*, vol. 9, pp. 2311–2344. Proc. Lunar Planet. Sci. Conf.

Hohenberg C. M., Hudson B., Kennedy B. M. and Podosek F. A. (1981) Xenon spallation systernatics in Angra dos Reis. *GCA* **45**, 1909–1915. https://doi.org/10.1016/0016-7037(81)90021-1.

Hohenberg C. M., Thonnard N. and Meshik A. (2002) Active capture and anomalous adsorption: new mechanisms for the incorporation of heavy noble gases. *Meteorit. Planet. Sci.* **37**, 257–267.

Humbert F., Libourel G., France-Lanord C., Zimmermann L. and Marty B. (2000) CO_2-laser extraction-static mass spectrometry analysis of ultra-low concentrations of nitrogen in silicates. *Geostandards Newsletter* **24**(2), 255–260.

Huss G. R., Ott U. and Kosheev A. P. (2008) Noble gases in presolar diamonds. III: Implications of ion implantation experiments with synthetic nanodiamonds. *Meteorit. Planet. Sci.* **43**, 1811–1826.

Jacobson S. A., Morbidelli A., Raymond S. N., O'brien D. P., Walsh K. J. and Rubie D. C. (2014) Highly siderophile elements in Earth/'s mantle as a clock for the Moon-forming impact. *Nature* **508**(7494), 84–87.

James O. B. (1980) Rocks of the early lunar crust. In *Proc. Lunar Planet. Sci. Conf*, vol. 11, pp. 365–393. Proc. Lunar Planet. Sci. Conf.

Koscheev A. P., Gromov M. D., Mohapatra R. K. and Ott U. (2001) History of traces gases in presolar diamonds inferred from ion-implantation experiments. *Nature* **412**, 615–617.

Kuga M., Marty B., Marrocchi Y. and Tissandier L. (2015) Synthesis of refractory organic matter in the ionized gas phase of the solar nebula. *Proc. Natl. Acad. Sci.* **112**(23), 7129–7134.

Lee J. Y., Marti K., Severinghaus J. P., Kawamura K., Yoo H. S., Lee J. B. and Kim J. S. (2006) A redetermination of the isotopic abundances of atmospheric Ar. *Geochim. Cosmochim. Acta* **70** (17), 4507–4512.

Leich D. A. and Niemeyer S. (1975) *Trapped xenon in lunar anorthositic breccia 60015*, pp. 1953–1965. Proc. Lunar Planet. Sci. Conf.

Leya I., Neumann S., Wieler R. and Michel R. (2001) The production of cosmogenic nuclides by galactic cosmic-ray particles for 2π exposure geometries. *Meteorit. Planet. Sci.* **36**, 1547–1561.

Lightner B. D. and Marti K. (1974) Lunar trapped xenon. In *Proc. Lunar Planet. Sci. Conf*, vol. 5, pp. 2023–2031. Proc. Lunar Planet. Sci. Conf.

Lugmair G. W. and Shukolyukov A. (1998) Early solar system timescales according to 53 Mn-53 Cr systematics. *Geochim. Cosmochim. Acta* **62**(16), 2863–2886.

Marrocchi Y. and Marty B. (2013) Experimental determination of the xenon isotopic fractionation during adsorption. *Geophys. Res. Lett.* **40**(16), 4165–4170.

Marrocchi Y., Marty B., Reinhardt P. and Robert F. (2011) Adsorption of xenon ions onto defects in organic surfaces: Implications for the origin and the nature of organics in primitive meteorites. *Geochim. Cosmochim. Acta* **75**(20), 6255–6266.

Marty B. (2012) The origins and concentrations of water, carbon, nitrogen and noble gases on earth. *Earth Planet. Sci. Lett.* **313–314**, 56–66.

Marty B. and Meibom A. (2007) Noble gas signature of the late heavy bombardment in the Earth's atmosphere. *EEarth* **2**(2), 43–49.

Marty B., Chaussidon M., Wiens R. C., Jurewicz A. J. G. and Burnett D. S. (2011) A ^{15}N-poor isotopic composition for the solar system as shown by Genesis solar wind samples. *Science* **332**(6037), 1533–1536.

Marty B., Avice G., Sano Y., Altwegg K., Balsiger H., Hässig M., Morbidelli A., Mousis O. and Rubin M. (2016) Origins of volatile elements (H, C, N, noble gases) on Earth and Mars in light of recent results from the ROSETTA cometary mission. *Earth Planet. Sci. Lett.* **441**, 91–102.

Marty B., Altwegg K., Balsiger H., Bar-Nun A., Bekaert D. V., Berthelier J. J., Bieler A., Briois C., Calmonte U., Combi M. and De Keyser J. (2017) Xenon isotopes in Comet 67P/Churyumov-Gerasimenko show comets contributed to Earth's atmosphere. *Science* **356**(6342), 1069–1072.

Meier M. M. M., Reufer A. and Wieler R. (2014) On the origin and composition of Theia: Constraints from new models of the Giant Impact. *Icarus* **242**, 316–328.

Meshik A., Hohenberg C., Pravdivtseva O. and Burnett D. (2014) Heavy noble gases in solar wind delivered by Genesis mission. *Geochim. Cosmochim. Acta* **127**, 326–347.

Meyer C. (2011) Lunar sample compendium.

Meyer C. (2012) Lunar sample compendium.

Meyer H. O. A. and McCallister R. H. (1973) Mineralogy and petrology of Apollo 16: Rock 60215, 13. In *Proc. Lunar Planet. Sci. Conf*, vol. 4, p. 661. Proc. Lunar Planet. Sci. Conf.

Michel T. and Eugster O. (1994) Primitive xenon in diogenites and plutonium-244-fission xenon ages of a diogenite, a howardite, and eucrites. *Meteoritics* **29**(5), 593–606.

Morbidelli A., Chambers J., Lunine J. I., Petit J. M., Robert F., Valsecchi G. B. and Cyr K. E. (2000) Source regions and timescales for the delivery of water to the Earth. *Meteorit. Planet. Sci.* **35**(6), 1309–1320.

Morbidelli A., Marchi S., Bottke W. F. and Kring D. A. (2012) A sawtooth-like timeline for the first billion years of lunar bombardment. *Earth Planet. Sci. Lett.* **355**, 144–151.

Moynier F., Albarède F. and Herzog G. F. (2006) Isotopic composition of zinc, copper, and iron in lunar samples. *Geochim. Cosmochim. Acta* **70**(24), 6103–6117.

Moynier F., Agranier A., Hezel D. C. and Bouvier A. (2010) Sr stable isotope composition of Earth, the Moon, Mars, Vesta and meteorites. *Earth Planet. Sci. Lett.* **300**(3), 359–366.

Niedermann S. and Eugster O. (1992) Noble gases in lunar anorthositic rocks 60018 and 65315: Acquisition of terrestrial krypton and xenon indicating an irreversible adsorption process. *Geochim. Cosmochim. Acta* **56**(1), 493–509.

Niemeyer S. and Leich D. A. (1976) Atmospheric rare gases in lunar rock 60015. In *Proc. Lunar Planet. Sci. Conf*, vol. 7, pp. 587–597. Proc. Lunar Planet. Sci. Conf.

Ong L., Asphaug E. I., Korycansky D. and Coker R. F. (2010) Volatile retention from cometary impacts on the Moon. *Icarus* **207**(2), 578–589.

Ozima M. and Podosek F. A. (2002) *Noble Gas Geochemistry*. Cambridge University Press.

Ozima M., Seki K., Terada N., Miura Y. N., Podosek F. A. and Shinagawa H. (2005) Terrestrial nitrogen and noble gases in lunar soils. *Nature* **436**(7051), 655–659.

Pepin R. (1994) The hunt for U-Xenon. *Meteoritics* **29**, 568.

Pepin R. O. and Phinney D. (1978) *Components of xenon in the solar system*. Space Science Center, University of Minnesota, p. 1.

Pepin R. O. and Porcelli D. (2002) Origin of noble gases in the terrestrial planets. *Rev. Mineral. Geochem.* **47**(1), 191–246.

Pepin R. O., Becker R. H. and Rider P. E. (1995) Xenon and krypton isotopes in extraterrestrial regolith soils and in the solar wind. *Geochim. Cosmochim. Acta* **59**(23), 4997–5022.

Pepin R. O., Schlutter D. J., Becker R. H. and Reisenfeld D. B. (2012) Helium, neon, and argon composition of the solar wind as recorded in gold and other Genesis collector materials. *Geochim. Cosmochim. Acta* **89**, 62–80.

Pahlevan K. and Stevenson D. J. (2007) Equilibration in the aftermath of the lunar-forming giant impact. *Earth Planet. Sci. Lett.* **262**(3), 438–449.

Ponganis K. V., Graf T. and Marti K. (1997) Isotopic fractionation in low-energy ion implantation. *J. Geophys. Res.* **102E**, 19335–19343.

Protin M., Blard P. H., Marrocchi Y. and Mathon F. (2016) Irreversible adsorption of atmospheric helium on olivine: A lobster pot analogy. *Geochim. Cosmochim. Acta* **179**, 76–88.

Pujol M., Marty B. and Burgess R. (2011) Chondritic-like xenon trapped in Archean rocks: a possible signature of the ancient atmosphere. *Earth Planet. Sci. Lett.* **308**(3), 298–306.

Raymond S. N., Quinn T. and Lunine J. I. (2004) Making other earths: Dynamical simulations of Terrestrial planet formation and water delivery. *Icarus* **168**, 1–17.

Reedy R. C. and Arnold J. R. (1972) Interaction of solar and galactic cosmic-ray particles with the Moon. *J. Geophys. Res.* **77**(4), 537–555.

Sano Y., Marty B. and Burnard P. (2013) Noble gases in the modern atmosphere. In *The Noble Gases as Geochemical Tracers* (ed. P. Burnard). Springer, Heidelberg, ISBN 978-3-642-28835-7, pp. 17–31.

Schaeffer O. A. and Husain L. (1974) Chronology of lunar basin formation and ages of lunar anorthositic rocks. In *Lunar Planet. Sci. Conf*, vol. 5, p. 663. Lunar Planet. Sci. Conf.

Scheiner S. (1997) *Hydrogen Bonding: A Theoretical Perspective*. Oxford University Press on Demand.

Sedaghatpour F., Teng F. Z., Liu Y., Sears D. W. and Taylor L. A. (2013) Magnesium isotopic composition of the Moon. *Geochim. Cosmochim. Acta* **120**, 1–16.

Signer P., Baur H., Derksen U., Etique P., Funk H., Horn P. and Wieler R. (1977) Helium, neon, and argon records of lunar soil evolution. In *Lunar and Planetary Science Conference Proceedings*, vol. 8, pp. 3657–3683. Lunar and Planetary Science Conference Proceedings.

Simon J. I. and DePaolo D. J. (2010) Stable calcium isotopic composition of meteorites and rocky planets. *Earth Planet. Sci. Lett.* **289**(3), 457–466.

Stettler A., Eberhardt P., Geiss J., Grogler N. and Maurer P. (1974) Sequence of terra rock formation and basaltic lava flows on the Moon. *Lunar Sci V*, 738–740.

Stuart B. (2005) *Infrared Spectroscopy*. John Wiley & Sons Inc.

Swindle T. D. and Kring D. A. (1997) Implications of small comets for the noble gas inventories of Earth and Mars. *Geophys. Res. Lett.* **24**(24), 3113–3116.

Terada K., Yokota S., Saito Y., Kitamura N., Asamura K. and Nishino M. N. (2017) Biogenic oxygen from Earth transported to the Moon by a wind of magnetospheric ions. *Nat. Astron.* **1**, 0026.

Thomson J. L. and Salisbury J. W. (1993) The mid-infrared reflectance of mineral mixtures (7–14 μm). *Remote Sens. Environ.* **45**(1), 1–13.

Vogel N., Heber V. S., Baur H., Burnett D. S. and Wieler R. (2011) Argon, krypton, and xenon in the bulk solar wind as collected by the Genesis mission. *Geochim. Cosmochim. Acta* **75**(11), 3057–3071.

Wiechert U. (2001) Oxygen isotopes and the Moon-forming event. *Science* **294**, 345–348.

Wieler R. (2002) Noble gases in the solar system. *Rev. Mineral. Geochem.* **47**(1), 21–70.

Wieler R. and Heber V. S. (2003) Noble gas isotopes on the Moon. *Space Sci. Rev.* **106**(1–4), 197–210.

Wieler R., Baur H. and Signer P. (1986) Noble gases from solar energetic particles revealed by closed system stepwise etching of lunar soil minerals. *Geochim. Cosmochim. Acta* **50**(9), 1997–2017.

Young E. D., Kohl I. E., Warren P. H., Rubie D. C., Jacobson S. A. and Morbidelli A. (2016) Oxygen isotopic evidence for vigorous mixing during the Moon-forming giant impact. *Science* **351**(6272), 493–496.

Zhang J., Dauphas N., Davis A. M., Leya I. and Fedkin A. (2012) The proto-Earth as a significant source of lunar material. *Nat. Geosci.* **5**(4), 251–255.

Zimmermann L. and Marty B. (2014) Méthodes d'extraction des gaz rares sous ultravide. *Techniques de l'ingénieur*, j6632.

Zimmermann L., Burnard P., Marty B. and Gaboriaud F. (2009) Laser ablation (193 nm), purification and determination of very low concentrations of solar wind nitrogen implanted in targets from the Genesis spacecraft. *Geostand. Geoanal. Res.* **33**(2), 183–194.

Associate editor: Alexander Nemchin